

Spectroscopic Observation of Helium-Ion- and Hydrogen-Catalyzed Hydrino Transitions

R. L. Mills, Y. Lu, K. Akhtar

BlackLight Power, Inc., 493 Old Trenton Road, Cranbury, NJ 08512

ABSTRACT

Mills [1-12] solved the structure of the bound electron using classical laws and subsequently developed a unification theory based on those laws called the Grand Unified Theory of Classical Physics (GUTCP) with results that match observations for the basic phenomena of physics and chemistry from the scale of the quarks to cosmos. In addition to the observables on the hydrogen atom that are known, it further predicts that atomic hydrogen may undergo a catalytic reaction with certain atomized elements and ions which singly or multiply ionize at integer multiples of the potential energy of atomic hydrogen, $m \cdot 27.2 \text{ eV}$ wherein m is an integer. The predicted reaction involves a resonant, nonradiative energy transfer from otherwise stable atomic hydrogen to the catalyst capable of accepting the energy. The product is $H(1/p)$, fractional Rydberg states of atomic hydrogen called "hydrino atoms" wherein $n = \frac{1}{2}, \frac{1}{3}, \frac{1}{4}, \dots, \frac{1}{p}$ ($p \leq 137$ is an integer) replaces the well-known parameter $n = \text{integer}$ in the Rydberg equation for hydrogen excited states. Two such atomic catalytic systems involve helium ions and two H atoms. The second ionization energy of helium is 54.4 eV ; thus, the ionization reaction of He^+ to He^{2+} has a net enthalpy of reaction of 54.4 eV which is equivalent to $2 \cdot 27.2 \text{ eV}$. Furthermore, the potential energy of atomic hydrogen is 27.2 eV such that two H atoms formed from H_2 by collision with a third, hot H can also act as a catalyst for this third H to cause the same transition as He^+ as the catalyst. The energy transfer is predicted to pump the He^+ ion energy levels and increase the electron excitation temperature of H in helium-hydrogen and hydrogen plasmas, respectively. Following the energy transfer to the catalyst the radius of the H atom is predicted to decrease as the electron undergoes radial acceleration to a stable state having a radius that is $1/3$ the radius of the uncatalyzed hydrogen atom with the further release of 54.4 eV of energy. This energy may be emitted as a characteristic EUV continuum with a cutoff at 22.8 nm and extending to longer wavelengths, or as third-body kinetic energy wherein a resonant kinetic-energy transfer to form fast H occurs. Subsequent excitation of these fast $H(n=1)$ atoms by collisions with the background species followed by emission of the corresponding $H(n=3)$ fast atoms is predicted to give rise to broadened Balmer α emission. The product $H(1/3)$ reacts rapidly to form $H(1/4)$, then molecular hydrino, $H_2(1/4)$, as a preferred state. Extreme ultraviolet (EUV) spectroscopy and high-resolution visible spectroscopy were recorded on microwave and glow and pulsed discharges of helium with hydrogen and hydrogen alone. Pumping of the He^+ ion lines occurred with the addition of hydrogen, and the excitation temperature of hydrogen plasmas under certain conditions was very high. Furthermore, for both plasmas providing catalysts He^+ and $2H$, respectively, the EUV continuum and extraordinary ($>50 \text{ eV}$) Balmer α line broadening were observed. $H_2(1/4)$ was observed by solution NMR at 1.25 ppm on gases collected from helium-hydrogen and water-

vapor-assisted hydrogen plasmas and dissolved in $CDCl_3$. Thus, we report the experimental confirmation of all four predictions for transitions of atomic hydrogen to form hydrinos. These results have profound implications theoretically, scientifically, and technologically in that they (1) confirm GUTCP in the prediction of hydrinos, (2) directly disprove atomic theories such as the Schrödinger and Dirac equations based on the definition of $n=1$ as the ground state, the defined state below which it is impossible to go, (3) offer resolution to many otherwise inexplicable celestial observations, and (4) directly demonstrate a new field of hydrogen chemistry and a powerful new energy source.

Key Words: helium-hydrogen and hydrogen plasmas, catalysis, pumping, $q \cdot 13.6 \text{ eV}$ EUV continua, fast hydrogen, molecular hydrino

I. Introduction

J. R. Rydberg showed that all of the spectral lines of atomic hydrogen were given by a completely empirical relationship:

$$\bar{\nu} = R \left(\frac{1}{n_f^2} - \frac{1}{n_i^2} \right) \quad (1)$$

where $R = 109,677 \text{ cm}^{-1}$, $n_f = 1, 2, 3, \dots$, $n_i = 2, 3, 4, \dots$ and $n_i > n_f$. Bohr, Schrödinger, and Heisenberg, each developed a theory for atomic hydrogen that gave the energy levels in agreement with Rydberg's equation.

$$E_n = -\frac{e^2}{n^2 8\pi\epsilon_0 a_H} = -\frac{13.598 \text{ eV}}{n^2} \quad (2a)$$

$$n = 1, 2, 3, \dots \quad (2b)$$

where e is the elementary charge, ϵ_0 is the permittivity of vacuum, and a_H is the radius of the hydrogen atom. The Rydberg equation is a simple integer formula that empirically represents the Rydberg series of spectral lines, the entire hydrogen spectrum given in terms of the differences between all of the principal energy levels of the hydrogen atom. Reproducing this equation was seen as validation of models proposed for the one-electron atom. The Bohr theory was the first success, but failed to physically predict the stability of the $n = 1$ state as well as the splitting of the spectral lines in a magnetic field and other atomic observables beyond the Rydberg series of lines. Consequently, Schrödinger proposed that the electron charge as a "cloud" obeyed a three-dimensional wave equation. This model was later modified by Born who proposed a point electron existing everywhere at once weighed statically so that only an expectation value as a single-valued observable is obtained with measurement that "collapses" the infinity of simultaneous values. This current model is untenable physically; rather, it is purely mathematical and relies on a mathematical definition for the stability of the $n = 1$ state [1, 4, 6-9, 11-12]. Consequently, it is disproved on mathematical inconsistency grounds by the existence of lower-states since the mathematics does not allow such states. In contrast to the current point-particle models that are physically flawed or not based on physics at all, Mills [1-12] solved the structure of the bound electron using classical laws. In closed-form equations containing fundamental constants only, this solution naturally and intuitively predicts the hydrogen-atom observables such as the stability of the $n = 1$ state and the instability of the excited states, the equation of the photon and electron in excited states, the resonant line width and shape, the selection rules, the correspondence principle, the magnetic moment of a Bohr magneton, the g factor, the Lamb shift, orbital and spin splitting, spin-orbit coupling (fine structure), and spin-nuclear coupling (hyperfine structure) in agreement with observation. Mills subsequently developed a unification theory based on the classical laws called the Grand Unified Theory of Classical Physics (GUTCP) with results that match observations for the basic phenomena of physics and chemistry from the scale of the quarks to cosmos. This paper is the second in a series of three that covers two specific predictions of GUTCP, two involving the existence of lower-energy states of the hydrogen atom and the transition mechanism, which represents a powerful new energy source, and the third the existence of a fifth force [2] beyond the electromagnetic, strong and weak-nuclear, and gravitational forces.

GUTCP predicts a reaction involving a resonant, nonradiative energy transfer from otherwise stable atomic hydrogen to a catalyst capable of accepting the energy to form hydrogen

in lower-energy states than previously thought possible. Specifically, the product is $H(1/p)$, fractional Rydberg states of atomic hydrogen wherein $n = \frac{1}{2}, \frac{1}{3}, \frac{1}{4}, \dots, \frac{1}{p}$ ($p \leq 137$ is an integer) replaces the well known parameter $n = \text{integer}$ in the Rydberg equation for hydrogen excited states. The excited energy states of atomic hydrogen are given by Eq. (2a) for $n > 1$ in Eq. (2b). The $n = 1$ state is the “ground” state for “pure” photon transitions (i.e. the $n = 1$ state can absorb a photon and go to an excited electronic state, but it cannot release a photon and go to a lower-energy electronic state). However, an electron transition from the ground state to a lower-energy state may be possible by a resonant nonradiative energy transfer such as multipole coupling or a resonant collision mechanism. Processes such as hydrogen molecular bond formation that occur without photons and that require collisions are common [13]. Also, some commercial phosphors are based on resonant nonradiative energy transfer involving multipole coupling [14].

The theory reported previously [1-12, 15] predicts that atomic hydrogen may undergo a catalytic reaction with certain atoms, excimers, ions, and diatomic hydrides which provide a reaction with a net enthalpy of an integer multiple of the potential energy of atomic hydrogen, $E_n = 27.2 \text{ eV}$ where E_n is one Hartree. Specific species identifiable on the basis of their known electron energy levels are required to be present with atomic hydrogen to catalyze the process. The reaction involves a nonradiative energy transfer followed by emission or energy transfer to H to form extraordinarily hot, excited-state H [15-22] and a hydrogen atom that is lower in energy than unreacted atomic hydrogen that corresponds to a fractional principal quantum number given by

$$n = 1, \frac{1}{2}, \frac{1}{3}, \frac{1}{4}, \dots, \frac{1}{p}; \quad p \leq 137 \text{ is an integer} \quad (2c)$$

in Eq. (1). The $n = 1$ state of hydrogen and the $n = \frac{1}{\text{integer}}$ states of hydrogen are nonradiative, but a transition between two nonradiative states, say $n = 1$ to $n = 1/2$, is possible via a nonradiative energy transfer. Thus, a catalyst provides a net positive enthalpy of reaction of $m \cdot 27.2 \text{ eV}$ (i.e. it resonantly accepts the nonradiative energy transfer from hydrogen atoms and releases the energy to the surroundings to affect electronic transitions to fractional quantum energy levels). As a consequence of the nonradiative energy transfer, the hydrogen atom becomes unstable and emits further energy until it achieves a lower-energy nonradiative state having a principal energy level given by Eqs. (2a) and (2c).

He^+ , $2H$, Ar^+ , Sr^+ , Li , K , Cs , and NaH are predicted to serve as catalysts since they meet the catalyst criterion—a chemical or physical process with an enthalpy change equal to an integer multiple of the potential energy of atomic hydrogen, 27.2 eV . The data from a broad spectrum of investigational techniques strongly and consistently support the existence of these states called hydrino, for “small hydrogen,” and the corresponding diatomic molecules called molecular hydrino. Some of these prior related studies supporting the possibility of a novel reaction of atomic hydrogen, which produces hydrogen in fractional quantum states that are at lower energies than the traditional “ground” ($n = 1$) state, include extreme ultraviolet (EUV) spectroscopy, characteristic emission from catalysts and the hydride ion products, lower-energy hydrogen emission, chemically-formed plasmas, Balmer α line broadening, population inversion of H lines, elevated electron temperature, anomalous plasma afterglow duration, power generation, and analysis of novel chemical compounds [15-45].

Recently, there has been the announcement of some unexpected astrophysical results that support the existence of hydrinos. In 1995, Mills published the GUTCP prediction [46] that the expansion of the universe was accelerating from the same equations that correctly predicted the mass of the top quark before it was measured. To the astonishment of cosmologists, this was confirmed by 2000. Mills made another prediction about the nature of dark matter based on GUTCP that may be close to being confirmed. Based on recent evidence, Bournaud et al. [47-48] suggest that dark matter is hydrogen in dense molecular form that somehow behaves differently in terms of being unobservable except by its gravitational effects. Theoretical models predict that dwarfs formed from collisional debris of massive galaxies should be free of nonbaryonic dark matter. So, their gravity should tally with the stars and gas within them. By analyzing the observed gas kinematics of such recycled galaxies, Bournaud et al. [47-4] have measured the gravitational masses of a series of dwarf galaxies lying in a ring around a massive galaxy that has recently experienced a collision. Contrary to the predictions of Cold-Dark-Matter (CDM) theories, their results demonstrate that they contain a massive dark component amounting to about twice the visible matter. This baryonic dark matter is argued to be cold molecular hydrogen, but it is distinguished from ordinary molecular hydrogen in that it is not traced at all by traditional methods, such as emission of CO lines. These results match the predictions of the dark matter being molecular hydrino.

Emission lines recorded on cold interstellar regions containing dark matter matched $H(1/p)$, fractional Rydberg states of atomic hydrogen given by Eqs. (2a) and (2c) [39]. Such emission lines with energies of $q \cdot 13.6 \text{ eV}$, where $q = 1, 2, 3, 4, 6, 7, 8, 9, \text{ or } 11$ were also observed by extreme ultraviolet (EUV) spectroscopy recorded on microwave discharges of helium with 2% hydrogen [37-39]. He^+ fulfills the catalyst criterion—a chemical or physical process with an enthalpy change equal to an integer multiple of 27.2 eV since it ionizes at 54.417 eV , which is $2 \cdot 27.2 \text{ eV}$. The product of the catalysis reaction of He^+ , $H(1/3)$, may further serve as a catalyst to lead to transitions to other states $H(1/p)$. These results also have further implications for the resolution of many celestial mysteries such as the paradox of the identity of dark matter, the identity of the radiation source behind the observation that diffuse $H\alpha$ emission is ubiquitous throughout the Galaxy and widespread sources of flux shortward of 912 \AA are required, the solar corona problem, the cause of sunspots and other solar activity, and why the Sun emits X-rays [39].

The highly energetic hydrino transition gives rise to five corresponding predicted characteristic signatures: (1) excess power, (2) emission of broad-band $q \cdot 13.6 \text{ eV}$ radiation, (3) pumping of the catalyst excited states, (4) characteristic EUV continuum radiation, (5) fast H, and (6) hydrino products. The first characteristic was reported on previously [32-33]. For a sufficiently high kinetics, the transitions to form hydrinos will produce measurable power. As predicted, water bath calorimetry showed $He/H_2(10\%)$ (500 mTorr) plasmas generated with an Evenson microwave cavity consistently yielded on the order of 50% more heat than the plasma control of He under identical conditions of gas flow, pressure, and microwave operating conditions corresponding to an excess power density of about $10 \text{ W} \cdot \text{cm}^{-3}$. In addition to unique vacuum ultraviolet (EUV) lines [37-39], He/H_2 plasmas also demonstrated dramatic broadening of the hydrogen Balmer series lines [15-22]. In this paper, we report on the nature of the latter four signatures of the hydrino transition and the conditions to reproducibly observe them.

The basis of each signature can be understood from a more detailed understanding of the

mechanism of the hydrino transition. Hydrogen is a special case of the stable states given by Eqs. (2a) and (2c) wherein the corresponding radius of the hydrogen or hydrino atom is given by

$$r = \frac{a_H}{p}, \quad (3)$$

where $p = 1, 2, 3, \dots$. In order to conserve energy, energy must be transferred from the hydrogen atom to the catalyst in units of

$$m \cdot 27.2 \text{ eV}, \quad m = 1, 2, 3, 4, \dots \quad (4)$$

and the radius transitions to $\frac{a_H}{m+p}$. Thus, the general reaction is given by

$$m \cdot 27.2 \text{ eV} + \text{Cat}^{q+} + H \left[\frac{a_H}{p} \right] \rightarrow \text{Cat}^{(q+r)+} + re^- + H \left[\frac{a_H}{(p+m)} \right] + [(p+m)^2 - p^2] \cdot 13.6 \text{ eV} \quad (5)$$

$$\text{Cat}^{(q+r)+} + re^- \rightarrow \text{Cat}^{q+} + m \cdot 27.2 \text{ eV} \quad (6)$$

And, the overall reaction is

$$H \left[\frac{a_H}{p} \right] \rightarrow H \left[\frac{a_H}{(p+m)} \right] + [(p+m)^2 - p^2] \cdot 13.6 \text{ eV} \quad (7)$$

q and r are integers.

As given *supra.*, helium is one of the catalysts that can cause a transition reaction because the second ionization energy is 54.4 eV , $m = 2$ in Eq. (4). Thus, the transition cascade for the p^{th} cycle is represented by

$$54.4 \text{ eV} + \text{He}^+ + H \left[\frac{a_H}{p} \right] \rightarrow \text{He}^{2+} + e^- + H \left[\frac{a_H}{(p+2)} \right] + [(p+2)^2 - p^2] \cdot 13.6 \text{ eV} \quad (8)$$

$$\text{He}^{2+} + e^- \rightarrow \text{He}^+ + 54.4 \text{ eV} \quad (9)$$

And, the overall reaction is

$$H \left[\frac{a_H}{p} \right] \rightarrow H \left[\frac{a_H}{(p+2)} \right] + [(p+2)^2 - p^2] \cdot 13.6 \text{ eV} \quad (10)$$

The reactions given by Eqs. (8-10) involve two steps of energy release: a nonradiative energy transfer to the catalyst followed by additional energy release as the radius decreases to the corresponding stable final state. Thus, the He^+ -catalyzed hydrino transition reaction may be written as follows:

$$54.4 \text{ eV} + \text{He}^+ + H \left[a_H \right] \rightarrow \text{He}^{2+} + e^- + H^* \left[\frac{a_H}{2+1} \right] + 54.4 \text{ eV} \quad (11)$$

$$H^* \left[\frac{a_H}{2+1} \right] \rightarrow H \left[\frac{a_H}{3} \right] + 54.4 \text{ eV} \quad (12)$$

$$\text{He}^{2+} + e^- \rightarrow \text{He}^+ + 54.4 \text{ eV} \quad (13)$$

And, the overall reaction is

$$H \left[a_H \right] \rightarrow H \left[\frac{a_H}{3} \right] + 54.4 \text{ eV} + 54.4 \text{ eV} \quad (14)$$

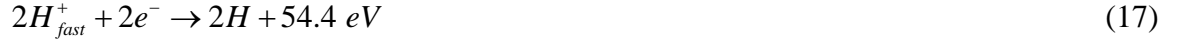
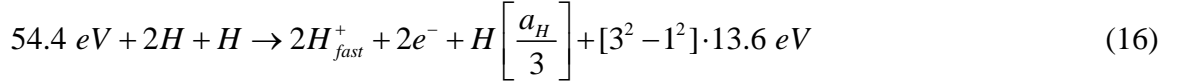
$H^* \left[\frac{a_H}{2+1} \right]$ has the radius of the hydrogen atom (corresponding to the 1 in the denominator) and a central field equivalent to 3 times that of a proton, and $H \left[\frac{a_H}{3} \right]$ is the corresponding stable state with the radius of 1/3 that of H. As the electron undergoes radial acceleration from the radius of the hydrogen atom to a radius of 1/3 this distance, energy is released as characteristic light emission or as third-body kinetic energy. The emission may be in the form of an extreme-ultraviolet continuum radiation having an edge at 54.4 eV (22.8 nm) and extending to longer wavelengths. Alternatively, H is the lightest atom; thus, it is the most probable fast species in collisional energy exchange from the H intermediate (e.g. $H^* \left[\frac{a_H}{2+1} \right]$). Additionally, H is unique with regard to the energetic transition state intermediate (generally represented by $H^* \left[\frac{a_H}{p+m} \right]$) in that all these species are energy states of hydrogen with corresponding harmonic frequencies. Thus, the cross section for H excitation by a nonradiative energy transfer to form fast H is predicted to be large since it is a resonant process. Efficient energy transfer can occur by common through-space mechanisms such as dipole-dipole interactions as described by Förster's theory [Chp. 6, Ref.1]. Consequently, in addition to radiation, a resonant kinetic energy transfer to form fast H may occur. Subsequent excitation of these fast $H(n=1)$ atoms by collisions with the background H_2 followed by emission of the corresponding $H(n=3)$ fast atoms gives rise to broadened Balmer α emission. Extraordinary (>100 eV) Balmer α line broadening is observed consistent with predictions [15-22].

Two hydrogen atoms may also serve as the catalyst. As given in Chp. 5 of Ref [1], and Refs. [15, 39], hydrogen atoms $H(1/p)$ $p=1,2,3,\dots,137$ can undergo further transitions to lower-energy states given by Eqs. (2a) and (2c) wherein the transition of one atom is catalyzed by a second that resonantly and nonradiatively accepts $m \cdot 27.2$ eV with a concomitant opposite change in its potential energy. The overall general equation for the transition of $H(1/p)$ to $H(1/(p+m))$ induced by a resonance transfer of $m \cdot 27.2$ eV to $H(1/p')$ is represented by

$$H(1/p') + H(1/p) \rightarrow H + H(1/(p+m)) + [2pm + m^2 - p^2 + 1] \cdot 13.6 \text{ eV} \quad (15)$$

Hydrogen atoms may serve as a catalyst wherein $m=1$ and $m=2$ for one and two atoms, respectively, acting as a catalyst for another. The rate for the two-atom-catalyst case would be appreciable only when the H density is high. But, high H densities are not uncommon. A high hydrogen atom concentration permissive of 2H serving as the energy acceptor for a third may be achieved under several circumstances such as on the surface of the Sun and stars due to the temperature and gravity driven density, on metal surfaces that support multiple monolayers, in highly dissociated plasmas, or in the case of a hydrogen molecule dissociating in the proximity of a hydrogen atom. The latter can occur commonly in a plasma having a large population of extraordinarily fast H as reported previously [15-22]. This is evidenced by the unusual intensity of atomic H emission. In such cases, energy transfer can occur from a hydrogen atom to two others within sufficient proximity, being typically a few angstroms [Chp 6 of Ref. 1]. Then, the

reaction between three hydrogen atoms whereby two atoms resonantly and nonradiatively accept 54.4 eV from the third hydrogen atom such that 2H serves as the catalyst is given by



And, the overall reaction is



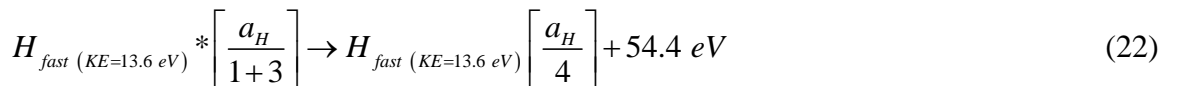
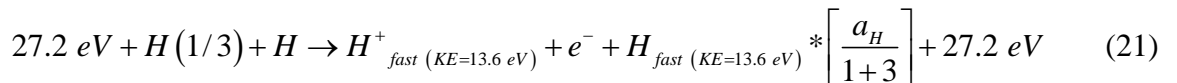
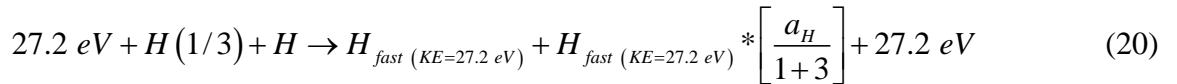
Since the $H * \left[\frac{a_H}{2+1} \right]$ intermediate of Eq. (16) is equivalent to that of Eqs. (8) and (11), the

continuum emission is predicted to be the same as that with He^+ as the catalyst. The energy transfer to two H causes pumping of the catalyst excited states, and fast H is produced directly as given by Eqs. (16-17) and by resonant kinetic energy transfer as in the case of He^+ as the catalyst. The EUV continuum radiation, pumping of H excited states, and fast H were also observed with hydrogen plasmas wherein 2H served as the catalyst.

The predicted product of the helium-ion and 2H catalyst reaction given by Eqs. (8-14) and Eqs. (16-18), respectively, is $H(1/3)$. In the case of a high hydrogen atom concentration, the further transition given by Eq. (15) of $H(1/3)$ ($p=3$) to $H(1/4)$ ($p+m=4$) with H as the catalyst ($p'=1$; $m=1$) can be fast:



A secondary continuum band is predicted arising from the subsequently rapid transition of the He^+ catalysis product $\left[\frac{a_H}{3} \right]$ (Eqs. (11-14)) to the $\left[\frac{a_H}{4} \right]$ state wherein atomic hydrogen accepts 27.2 eV from $\left[\frac{a_H}{3} \right]$. Consider the reactions given by Eqs. (16) and (19). Conservation of energy and linear momentum permits the formation of two hot intermediates, a hot $H_{fast (KE=13.6 \text{ eV})} * \left[\frac{a_H}{1+3} \right]$ intermediate having a kinetic energy (KE) of 13.6 eV and a hot $H_{fast (KE=27.2 \text{ eV})} * \left[\frac{a_H}{1+3} \right]$ intermediate having a kinetic energy (KE) of 27.2 eV. The intermediates having 54.4 and 40.8 eV of remaining energy can each further emit this energy as a continuum band starting at 22.8 nm and 30.4 nm, respectively, and continuing to longer wavelengths.



$$H_{fast (KE=27.2 eV)} * \left[\frac{a_H}{1+3} \right] \rightarrow H_{fast (KE=27.2 eV)} \left[\frac{a_H}{4} \right] + 40.8 eV \quad (23)$$

And, with thermalization, the overall reaction is

$$H(1/3) \rightarrow H \left[\frac{a_H}{4} \right] + [4^2 - 3^2] \cdot 13.6 eV \quad (24)$$

In addition, the collision of the intermediate of Eq. (20) with a helium atom to excite the dominant transition, $He(1s^2) + 21.21 eV \rightarrow He(1s^1 2p^1)$, gives rise to 63.3 nm emission via the following mechanism:

$$H_{fast (KE=27.2 eV)} * \left[\frac{a_H}{1+3} \right] + He(1s^2) \rightarrow H_{fast (KE=27.2 eV)} \left[\frac{a_H}{1+3} \right] + He(1s^1 2p^1) + h\nu(19.59 eV, 63.3 nm) \quad (25)$$

And, with thermalization and relaxation, the overall reaction is given by Eq. (24).

$H(1/4)$ and the corresponding molecular hydrino $H_2(1/4)$ are favored products as shown previously [15]. The NMR of catalysis-product gas provides a definitive test of the theoretically predicted chemical shift of $H_2(1/4)$. In general, the 1H NMR resonance of $H_2(1/p)$ is predicted to be upfield from that of H_2 due to the fractional radius in elliptic coordinates [1, 6] wherein the electrons are significantly closer to the nuclei. The predicted shift, $\frac{\Delta B_T}{B}$, for $H_2(1/p)$ derived previously [1, 6] is given by the sum of that of H_2 and a term that depends on $p = \text{integer} > 1$ for $H_2(1/p)$:

$$\frac{\Delta B_T}{B} = -\mu_0 \left(4 - \sqrt{2} \ln \frac{\sqrt{2} + 1}{\sqrt{2} - 1} \right) \frac{e^2}{36a_0 m_e} (1 + \pi c \rho) \quad (26)$$

$$\frac{\Delta B_T}{B} = -(28.01 + 0.64 p) ppm \quad (27)$$

where for H_2 $p = 0$. The experimental absolute H_2 gas-phase resonance shift of -28.0 ppm [49-52] is in excellent agreement with the predicted absolute gas-phase shift of -28.01 ppm (Eq. (27)).

Thus, in this paper, we report on the experimental confirmation of the four additional predictions of the physical mechanism to form hydrinos and means to readily reproduce them. We found a dependence of each signature on the plasma conditions with the observation of the pumping of the catalyst states in highly collisional, weakly ionized microwave plasma, fast H in weakly ionized plasma having a high-energy electron component to excite fast H before it cooled, and the characteristic EUV continuum radiation in diffuse, highly ionized pulsed discharge plasmas. Helium-hydrogen microwave plasmas have substantial He^+ and H emission and served as sources of $H_2(1/4)$ that was liquefied by a liquid helium trap to collect it over time. Hydrogen microwave plasmas were found to produce $H_2(1/4)$ at a slow rate possibly due to the lack of substantial fast H and low H concentrations due to a rapid wall recombination rate and a slow rate of dissociation since the electron temperature is low ($< 1 eV$) with the absence of a high-energy population. In order to achieve a 2H catalyst reaction involving a binary collision, it is necessary to first form fast H. It was reported previously that a high concentration of atomic H is formed in a water vapor RF cell [20] wherein several

monolayers of atomic H can initially form on the cathode surface to initiate the catalysis reaction [53-56]. On the contrary, the prevention of the formation of surface atomic hydrogen prevents the catalysis reaction [57]. Furthermore, it is known that water vapor may be added to the plasma to increase the hydrogen concentration [58]. Fast H in the gas phase can then advance the rate, and in addition to H, hydridinos undergoing increasingly energetic transitions to lower states can increase the energy of the fast H. From the width of the emitted 656.3 nm Balmer α line, it was previously found that capacitively coupled radio frequency (rf) water vapor plasmas in static mode (no-flow condition) showed two populations of atomic hydrogen. A typical slow population was observed that was independent of time, and a new phenomenon, an extraordinary fast population (130–150 eV) that increases to a significant portion of the Balmer α emission with time, was also observed. Thus, RF water vapor plasmas were batch-mode run in a cell with a diode configuration having two parallel large circular stainless steel electrodes as a source of H_2 (1/4) gas that was directly collected by liquefaction in an NMR solvent at 4 K.

II. Experimental

Microwave Emission Spectra. The experimental set up comprised a microwave discharge gas cell light source and an EUV spectrometer which was differentially pumped as described previously [37-39]. Extreme ultraviolet emission spectra were obtained on microwave plasmas of helium alone, helium-hydrogen (5% to 17%) mixtures, helium-nitrogen (5% to 17%) mixtures, and water vapor [44-45]. The microwave generator was a Sairem (GMP03KS, 2.45 GHz, 300W). The output power was set at 40 watts. Each gas was flowed through a half-inch diameter quartz tube at 1 Torr. The gas pressure inside the cell was maintained by flowing the gas while monitoring the pressure with a 10 Torr MKS Baratron absolute pressure gauge. The tube was fitted with an Sairem coaxial microwave cavity (Evenson cavity). The EUV spectrometer a McPherson grazing incidence EUV spectrometer (Model 248/310G) equipped with a grating having 600 lines/mm. The angle of incidence was 87° . The wavelength region covered by the monochromator was 5–65 nm. An aluminum filter (150 nm thick, band-pass 17–80 nm) was used to eliminate longer wavelength photons. The wavelength resolution was about 0.05 nm (FWHM) with an entrance slit width of 4 μm . The increment was 0.02 nm and the dwell time was 30–50 μm . The light was detected by a CEM.

Pulsed-Plasma Emission Spectra. EUV spectroscopy was recorded on argon, helium-hydrogen (98/2%), and hydrogen high-voltage pulsed discharge plasmas with the McPherson grazing incidence EUV spectrometer (Model 248/310G) using the same parameters as those of the microwave plasma spectra. The experimental set up is shown in Figure 1. A summary of high-voltage pulsed plasma parameters to observe the EUV continuum from hydridino transitions is given in Table 1. An electron gun (Commercial TV gun, Clinton Electronics Corporation, Model 3-659), driven by a high voltage pulse generator (DEI, GRX high voltage pulse generator), provides a pulsed electron beam with a beam voltage of 1-3 kV and a duration of 5-20 ms. The electron beam triggered a high voltage pulsed discharge at a repetition rate of 5 Hz. A negative high voltage power supply (Universal Voltronics Corp., Model 1650R2) was used to apply ~12 kV to the cathode of the main discharge. The main discharge cell comprised a tapered hollow anode (3 mm bore) and a hollow cathode (3 mm bore). The electrodes were separated by a 4 mm gap. Ultrahigh purity hydrogen, argon, helium-argon (90/10%) mixture, and helium-hydrogen (98/2%) mixture were flowed at rates between 1 to 10 sccm and pressures between 100 mTorr and 900 mTorr controlled by a mass flow controller (MKS, M100B21CG1BB). The

argon was added to the helium-only control to stabilize the helium plasma by providing an atom with a considerably lower ionization potential.

DC-Plasma and RF Emission Spectra. The width of the 656.3 nm Balmer α line emitted from H_2 , He/H_2 (95/5%), and Xe/H_2 (95/5%)-mixture plasmas was measured with a high resolution visible spectrometer capable of a resolution of ± 0.006 nm over the spectral range 190-860 nm. The DC glow-discharge light source comprised fine-tip, 2% thoriated tungsten electrodes of 3 mm diameter inside a 1.25 cm diameter quartz tube as shown in Figure 2. The electrodes were spaced 2 cm apart except where indicated for the study of the line-width dependence on the applied electric field. The very fine electrode tips were used primarily to minimize the surface area of the electrodes so that ions accelerated along the electric-field lines could not bounce off of the surface in the reverse direction. High-resolution plasma emission spectroscopy was performed along the electric field lines (end-on) and perpendicular to the field lines (side-on). For side-on observation an axial scan of the plasma emission along the cathode rod was also obtained. Here, the axial distance along the cathode is defined with the cathode tip located at $z=0$ cm as shown in Figure 2. In order to sample plasma emission looking towards the anode as well as the cathode for the end-on observation the polarity of the powered electrode was reversed.

The plasma chamber was evacuated using a scroll pump. The gas was introduced into the evacuated chamber using mass flow controller. The discharge pressure was maintained in the range of 0.01 Torr to 10 Torr by controlling the flow and pumping rate. A stabilized DC power supply (0-1 A and 0-600 V) was used to maintain the plasma. High-wattage current-limiting resistors of 200 Ω were used in series with the power supply and generator. Following breakdown, the glow discharge was maintained with cathode-anode voltages and currents in the ranges of 300-620 V and 10-100 mA, respectively, depending upon the gas pressure, gas flow, and discharge configuration.

The width of the 656.3 nm Balmer α line and high resolution visible (400–700 nm) spectra were also recorded on the emission from capacitively-coupled rf discharges of water vapor, water vapor with hydrogen and oxygen mixtures, pure hydrogen, oxygen-hydrogen mixtures, argon-hydrogen mixtures, and xenon–hydrogen mixtures according to methods reported previously [20]. The experimental set up shown in Figure 3 consisted of a large cylindrical quartz plasma chamber (14 cm ID \times 36 cm length) with a diode configuration in which the plasma was confined between two parallel circular stainless steel electrodes (0.1 mm thick \times 7.6 cm diameter with a 2 cm separation). 13.56 MHz radio frequency power (RF Power Products Inc. NJ, Model RF 5, 500 Watts) was coupled to the electrode using a commercially available impedance matching network (RF VII Inc., Glassboro, NJ). Radio frequency power from the impedance matchbox was fed to the capacitive electrodes using a 1/2-inch diameter steel tube that also facilitated the end-on (parallel to the electric field) observation of plasma through holes in the center of the electrodes. One of the electrodes was grounded (held constantly at $V=0$). A common ground was obtained for the grounded electrode, rf shield, and vacuum system. The impedance matching network was tuned to ensure that the reflected power was always less than 5% of the forward power. The applied rf voltage $V_{rf}(t)$ and current $I_{rf}(t)$ signals were measured at the powered electrode as described previously [20]. Two perpendicular ports in the center of the plasma chamber (Position 2) permitted side-on observations of plasma emission perpendicular to the electric field between the plates and placement of a Langmuir probe for plasma density and electron temperature measurement as described previously [20].

Plasma emission far away (15 cm) from the high-field plasma sheath region was sampled at Position 1 and Position 3.

A helium leak detector (QualyTest, Model: HLT 260, Pfeiffer Vacuum) was utilized to leak test the evacuated plasma chamber. The quartz plasma chamber pressure was maintained with a leak rate below 10^{-7} Torr-L/s, a very important requirement for experiments performed in no flow (static) condition. Independent mass flow controllers (MKS) were used to introduce water vapor, UHP grade (99.999%) H_2 , O_2 , Ar, and xenon gases into the plasma chamber through Ultratorr fittings close to the grounded electrode. A MKS Baratron gauge was used to read the chamber pressure. The vapor pressure of water at room temperature was sufficient to provide operating pressure in the chamber. In the static mode (no-flow mode), water vapor was leaked into the evacuated plasma chamber to the desired pressure with the vacuum pump valve closed.

The Balmer line widths were measured using a high-resolution visible spectrometer. The plasma emission was fiber-optically coupled to a Jobin Yvon Horiba 1250 M spectrometer described previously [16, 20] through a high-quality UV (200-800 nm) fiber-optic bundle and an 220F matching fiber adapter with an aperture of 0.12 and a corresponding acceptance angle of 12° . The spectrometer had a 1250 mm focal length with a 2400 g/mm grating and a detector comprising a photomultiplier tube (PMT) with a stand-alone power supply of 995 volts or a Symphony model, liquid-nitrogen cooled, back illuminated 2048×512 CCD array with an element size of $13.5 \mu\text{m} \times 13.5 \mu\text{m}$, 16 bit ADC, and 20 KHz and 1 MHz read outs. Using the 546 nm Hg I line from NIST calibrated mercury lamp with the entrance and exit slits set to 20 μm , the measured CCD resolution due to the finite-pixel-spectral width was very high, ± 0.006 nm. The spectrometer accuracy was ± 0.05 nm, and its repeatability was ± 0.005 nm. The spectrometer was scanned through the emission profiles helium atom, helium ion, and the Balmer lines with a step size of 0.01 nm at entrance and exit slit-widths of 20 μm .

The hydrogen atom Doppler energies were calculated from the width of the 656.3 nm Balmer α line emitted from the DC plasmas [59]. Each Balmer α spectral line was fit using one or two Gaussian curves: one for the “cold” (<1 eV) hydrogen and the second for “hot” (>10 eV) hydrogen. The full half-width $\Delta\lambda_G$ of each Gaussian results from the Doppler ($\Delta\lambda_D$) and instrumental ($\Delta\lambda_I$) half-widths:

$$\Delta\lambda_G = \sqrt{\Delta\lambda_D^2 + \Delta\lambda_I^2} \quad (28)$$

The measured half-width $\Delta\lambda_I$ of ± 0.006 nm was negligible. Thus, the temperature was calculated from the Doppler half-width using the formula:

$$\Delta\lambda_D = 7.16 \times 10^{-7} \lambda_0 \left(\frac{T}{\mu} \right)^{1/2} \quad (29)$$

where λ_0 is the line wavelength, T is the temperature in K ($1 \text{ eV} = 11,605 \text{ K}$), and μ is the molecular weight (=1 for atomic hydrogen). In each case, the error in the average Doppler half-width over 5 scans was about $\pm 5\%$ that was attributed predominately to fluctuations in the plasma.

In addition, $T_{excitation}$ was measured on DC discharge plasmas of hydrogen from the ratio of the intensity of the Balmer lines, and $T_{excitation}$ was measured on DC glow discharge plasmas of helium-hydrogen mixture (90/10)% from the ratio of the intensity of the He atomic lines as described by previously [17-18]. The electron density n_e and temperature T_e were determined using a Langmuir probe according to the method given previously [15, 18, 20].

NMR of Product H_2 (1/4) From Liquid-Helium Trapped He/H₂ Microwave Plasma Gases and Water-Vapor RF-Plasma Gases. Condensable gas from helium-hydrogen (90/10%) microwave plasmas maintained in an Evenson cavity was collected in a high-vacuum (10^{-6} Torr) capable, stainless steel, liquid helium (LHe) cryotrap as describe previously [23]. After each plasma run the cryotrap was pumped down to 10^{-5} Torr to remove any non-condensable gases in the system, and the ultrahigh-purity plasma gases were passed through a liquid nitrogen trap before flowing into the plasma cavity. Sealed 1H NMR samples were prepared by collecting the condensed gas from the cryotrap in $CDCl_3$ solvent (99.99% Cambridge isotopes) in an NMR tube (5 mm OD, 23 cm length, Wilmad) maintained at LHe-temperature which was sealed with a valve, removed form LHe, and then flame-sealed. Control NMR samples comprised starting gases of ultrahigh purity hydrogen (Praxair) and the helium-hydrogen (90/10%) mixture with $CDCl_3$ solvent and plasma gas of helium alone. The NMR spectra were recorded with a 500 MHz Bruker NMR spectrometer that was deuterium locked. The chemical shifts were referenced to the external tetramethylsilane (TMS). Gases from the water-vapor RF plasma showing fast H were also analyzed by solution NMR wherein the plasma gases were condensed in the NMR tube immersed in LHe.

III. Results and Discussion

A. Microwave Emission Spectra and $T_{excitation}$ Measurements. The emission spectrum (25-60 nm) of the helium-alone microwave plasma recorded by the EUV grazing incidence spectrometer is shown in Figure 4. Essentially only helium atomic lines were observed with the $1s^1 2p^1 \rightarrow 1s^2$ transition being dominant. The insert (20-45 nm region) shows weak helium ion lines in the normal intensity ratios as a Rydberg series. The dominance of the atomic over the ionic lines is evident by the intensity relationship of $58.4 \text{ nm} \gg 30.4 \text{ nm}$. When a small amount of hydrogen was added the spectrum changed dramatically in a manner that is inexplicable based on known plasma phenomena (Figure 5). Specially, a reversal of the intensity relationship of the atomic and the ionic lines occurred as evident by the intensity relationship of $58.4 \text{ nm} \ll 30.4 \text{ nm}$. Essentially only helium ion lines were observed with the $2p^1 \rightarrow 1s^1$ transition being dominant. The addition of hydrogen did not cause the plasma to become optically thick since the 58.4 nm line intensity remained essentially unchanged while the helium ion lines increase over fourteen fold with the introduction of 17% hydrogen. Furthermore, it was observed that the relative atomic to ionic line intensities remained the same with the introduction of 17% nitrogen that has very similar absorption characteristics. Thus, the hydrino transition reaction initiated by the addition of hydrogen was evident by the predicted pumping of the He^+ lines.

The same phenomenon was also observed in the case of the $2H$ catalyst as reported previously [44-45]. The pumping of the H lines to extraordinarily high levels demonstrated that the $2H$ catalyst served to maintain a high hydrino transition reaction rate in a water-vapor microwave discharge plasma. Specifically, the hydrogen Balmer lines corresponding to the transitions from the n th principal quantum level beyond the 16^{th} state to the $n=2$ level were observed as shown in Figure 6.

The reversal of the intensity relationship of the atomic and the ionic lines in helium microwave plasmas with the addition of hydrogen and the pumping of the H-excited states in water-vapor plasmas corresponded to high excitation temperatures wherein He^+ and $2H$ served as the catalyst, respectively. The excitation temperature $T_{excitation}$ for both helium-hydrogen and

water-vapor plasmas was between 2.5 and 3 eV when the highly excited state populations were observed compared to the ordinary-state value of about 1 eV. Thus, the predicted pumping of the catalyst excited-state energy levels due to the energy transfer from H to the catalyst was observed.

B. Pulsed-Plasma Emission Spectra. Argon was run as a control since the corresponding transition of the intermediate, $H * \left[\frac{a_H}{2} \right] \rightarrow H \left[\frac{a_H}{2} \right] + 13.6 \text{ eV}$, with Ar^+ as the catalyst gives rise to a continuum beyond the measured spectral range such that, even with hydrogen contamination, a continuum in the region of 20 or 30 nm was not predicted. The results confirm expectations as shown in Figure 7. Helium without hydrogen and ~10% argon added to stabilize the plasma was also run as shown in Figure 8. Only known helium ion lines were observed in the absence of a continuum.

In contrast, the predicted continua were observed with He^+ as the catalyst. The emission spectrum of an electron-beam-initiated, high-voltage pulsed discharge in a helium-hydrogen mixture (98/2%), recorded by the EUV grazing incidence spectrometer is shown in Figure 9. The predicted continua from the transition $H * \left[\frac{a_H}{3} \right] \rightarrow H \left[\frac{a_H}{3} \right] + 54.4 \text{ eV}$ and

$H_{fast (KE=27.2 \text{ eV})} * \left[\frac{a_H}{4} \right] + \rightarrow H \left[\frac{a_H}{4} \right] + 40.8 \text{ eV}$ were observed with a cutoff at 22.8 nm and 30.4 nm, respectively, with the intensity increasing to a maximum at longer wavelengths. In contrast, no continuum is ordinarily observed as shown by the helium ion Rydberg series in Figures 4 and 5 and with controls argon and helium with 10% argon as shown in Figures 7 and 8, respectively. Additionally, only helium ion lines were observed on top of the continuum to the cutoff of the Rydberg series at 22.8 nm. Similarly, the same continuum was observed with hydrogen as shown in the emission spectrum of an electron-beam-initiated, high-voltage pulsed discharge in hydrogen, recorded by the EUV grazing incidence spectrometer (Figure 10). These results cannot be explained by conventional mechanisms. Ion recombination known to produce a continuum gives a characteristic “wedge” on a logarithmic plot of intensity versus wavelength wherein the electron temperature can be determined from the slope. The first continuum has a discontinuity at the threshold ionization energy at of 54.4 eV at 22.8 nm, but the intensity is a maximum at the threshold and decreases exponentially to shorter wavelengths due to conservation of the energy of the recombination and the electron kinetic energy. This type of continuum is a bound-free type; whereas, that of the hydrino transition is of the free-free type such as that of the hydride ion having an increasing intensity to longer wavelengths from the limit of zero intensity at the threshold. Only the hydrino transition produces a free-free continuum in the EUV. Furthermore, hydrogen has no recombination threshold at 22.8 nm nor at 30.4 nm, and, in fact, has no lines in the EUV region at all.

Bremsstrahlung was also eliminated since the intensity is observed to form a broad peak at a very high energy (~51.7 eV, 24 nm) for the first continuum; whereas, Bremsstrahlung radiation has an intensity profile that exponentially decays from the long-wavelength region [60]. Additionally, molecules cannot emit in this energy region and were eliminated from consideration. Only atomic and ionic emission is possible at these energies corresponding to line emission, and no continuum emission is possible even for Doppler broadened lines. From Wien’s displacement law, blackbody radiation at 24 nm wavelengths would correspond to a

temperature of $1.2 \times 10^5 \text{ K}$, an absolutely impossible scenario. Thus, the lines are assigned to predicted $q \cdot 13.6 \text{ eV}$ continua with thresholds at 54.4 eV ($q = 4$) and 40.8 eV ($q = 3$) for He^+ catalyst.

Similarly to the case of He^+ , argon ions can provide a net enthalpy of a multiple of that of the potential energy of the hydrogen atom, but the transition is to a different state. Rather than 54.4 eV , the second ionization energy of argon is 27.63 eV . Then, the reaction Ar^+ to Ar^{2+} has a net enthalpy of reaction of 27.63 eV , which is equivalent to $m = 1$ in Eqs. (4-7).

$$27.63 \text{ eV} + \text{Ar}^+ + \text{H}[a_H] \rightarrow \text{Ar}^{2+} + e^- + \text{H}^* \left[\frac{a_H}{1+1} \right] + 27.2 \text{ eV} \quad (30)$$

$$\text{H}^* \left[\frac{a_H}{1+1} \right] \rightarrow \text{H} \left[\frac{a_H}{2} \right] + 13.6 \text{ eV} \quad (31)$$

$$\text{Ar}^{2+} + e^- \rightarrow \text{Ar}^+ + 27.63 \text{ eV} \quad (32)$$

And, the overall reaction is

$$\text{H}[a_H] \rightarrow \text{H} \left[\frac{a_H}{2} \right] + 27.2 \text{ eV} + 13.6 \text{ eV} \quad (33)$$

The emission may be in the form of an extreme-ultraviolet continuum radiation having an edge at 13.6 eV (91.2 nm) and extending to longer wavelengths. Alternatively, resonant kinetic energy transfer from $\text{H}^* \left[\frac{a_H}{2} \right]$ to background H to form fast H may occur. Subsequent excitation of these fast $\text{H}(n=1)$ atoms by collisions with the background H_2 followed by emission of the corresponding $\text{H}(n=3)$ fast atoms gives rise to broadened Balmer α emission. Extraordinary ($>100 \text{ eV}$) Balmer α line broadening is observed consistent with predictions [15-22].

A secondary continuum band is also predicted for Ar^+ arising from the subsequently rapid transition of the Ar^+ catalysis product $\left[\frac{a_H}{2} \right]$ (Eqs. (30-33)) to the $\left[\frac{a_H}{3} \right]$ state wherein atomic hydrogen accepts 27.2 eV from $\left[\frac{a_H}{2} \right]$. The corresponding two hot intermediates are

$\text{H}_{fast (KE=13.6 \text{ eV})}^* \left[\frac{a_H}{1+2} \right]$ having a kinetic energy (KE) of 13.6 eV and $\text{H}_{fast (KE=27.2 \text{ eV})}^* \left[\frac{a_H}{1+2} \right]$ having a kinetic energy (KE) of 27.2 eV . The intermediates having 27.2 eV and 13.6 eV of remaining energy can each further emit this energy as a continuum band starting at 45.6 nm and 91.2 nm , respectively, and continuing to longer wavelengths.

$$27.2 \text{ eV} + \text{H}(1/2) + \text{H} \rightarrow \text{H}_{fast (KE=27.2 \text{ eV})} + \text{H}_{fast (KE=27.2 \text{ eV})}^* \left[\frac{a_H}{1+2} \right] + 27.2 \text{ eV} \quad (34)$$

$$27.2 \text{ eV} + \text{H}(1/2) + \text{H} \rightarrow \text{H}_{fast (KE=13.6 \text{ eV})}^+ + e^- + \text{H}_{fast (KE=13.6 \text{ eV})}^* \left[\frac{a_H}{1+2} \right] + 27.2 \text{ eV} \quad (35)$$

$$\text{H}_{fast (KE=27.2 \text{ eV})}^* \left[\frac{a_H}{1+2} \right] \rightarrow \text{H}_{fast (KE=27.2 \text{ eV})} \left[\frac{a_H}{3} \right] + 13.6 \text{ eV} \quad (36)$$

$$H_{fast (KE=13.6 eV)} * \left[\frac{a_H}{1+2} \right] \rightarrow H_{fast (KE=13.6 eV)} \left[\frac{a_H}{3} \right] + 27.2 eV \quad (37)$$

And, with thermalization, the overall reaction is

$$H(1/2) \rightarrow H \left[\frac{a_H}{3} \right] + [3^2 - 2^2] \cdot 13.6 eV \quad (38)$$

With the additional insight into the nature of hydrino transitions, the primary and secondary EUV continua predicted by Eqs. (31) and (37) are reasonably identifiable in previously reported spectra [41]. A signature of the energetic hydrino transition process is the formation of a plasma called a resonant transfer- or rt-plasma at low temperatures (e.g. $\approx 10^3 K$) and very low field strengths of about 1-2 V/cm when a catalyst present with atomic hydrogen. As shown in Figures 17 and 31 of Ref. [41] continua bands starting at 45.6 nm and 91.2 nm and continuing to longer wavelengths were recorded on an rt-plasma having Ar^+ as the catalyst. Other sources of continua can be eliminated. Molecular hydrogen band were not observed in the 90 nm to 130 nm region, nor were they observed in the 140-160 nm region as shown in Figure 31. Only Ar , Ar^+ , and H lines were observed in Figure 17, and additionally Cs and Cs^+ lines were observed in Figure 31. Argon excimer continua emit in longer wavelength regions [23], and no continua are possible in the region of the secondary continuum having a threshold of 45.6 nm. Considering these results and those of helium plasmas, the $q \cdot 13.6 eV$ continua with thresholds at 54.4 eV ($q=4$) and 40.8 eV ($q=3$) for He^+ catalyst and at 27.2 eV ($q=2$) and 13.6 eV ($q=1$) for Ar^+ catalyst have been observed. Much higher values of q are possible with transitions of hydrinos to lower states giving rise to high-energy continuum radiation over a broad spectral region as reported previously [39]. These results have further implications for the resolution of many celestial mysteries such as the paradox of the identity of dark matter and the identity of the radiation source behind the observation that diffuse $H\alpha$ emission is ubiquitous throughout the Galaxy and widespread sources of flux shortward of 912 Å are required [39].

The Universe is predominantly comprised of hydrogen and a small amount of helium. These elements exist in interstellar regions of space, and they are expected to comprise the majority of interstellar matter. However, the observed constant angular velocity of many galaxies as the distance from the luminous galactic center increases can only be accounted for by the existence of nonluminous weakly interacting matter, dark matter. It was previously accepted that dark matter exists at the cold fringes of galaxies and in cold interstellar space. This has since been disproved by the observation of Bournaud et al. [47-48] that demonstrated that galaxies are mostly comprised of dark matter, and the data persistently supports that dark matter probably accounts for the majority of the universal mass.

The identity of dark matter has been a cosmological mystery. It is anticipated that the emission spectrum of the extreme ultraviolet background of interstellar matter possesses the spectral signature of dark matter. Labov and Bowyer designed a grazing incidence spectrometer to measure and record the diffuse extreme ultraviolet background [61]. The instrument was carried aboard a sounding rocket, and data were obtained between 80 Å and 650 Å (data points approximately every 1.5 Å). Several lines including an intense 635 Å emission associated with dark matter were observed [61] which has considerable astrophysical importance as indicated by the authors:

“Regardless of the origin, the 635 Å emission observed could be a major source of

ionization. Reynolds (1983, 1984, 1985) has shown that diffuse $H\alpha$ emission is ubiquitous throughout the Galaxy, and widespread sources of flux shortward of 912 \AA are required. Pulsar dispersion measures (Reynolds 1989) indicate a high scale height for the associated ionized material. Since the path length for radiation shortward of 912 \AA is low, this implies that the ionizing source must also have a large scale height and be widespread. Transient heating appears unlikely, and the steady state ionization rate is more than can be provided by cosmic rays, the soft X-ray background, B stars, or hot white dwarfs (Reynolds 1986; Brushweiler & Cheng 1988). Sciama (1990) and Salucci & Sciama (1990) have argued that a variety of observations can be explained by the presence of dark matter in the galaxy which decays with the emission of radiation below 912 \AA .

The flux of 635 \AA radiation required to produce hydrogen ionization is given by $F = \zeta_H / \sigma_\lambda = 4.3 \times 10^4 \zeta_{-13} \text{ photons cm}^{-2} \text{ s}^{-1}$, where ζ_{-13} is the ionizing rate in units of 10^{-13} s^{-1} per H atom. Reynolds (1986) estimates that in the immediate vicinity of the Sun, a steady state ionizing rate of ζ_{-13} between 0.4 and 3.0 is required. To produce this range of ionization, the 635 \AA intensity we observe would have to be distributed over 7% - 54% of the sky.”

The $63.5 \pm 0.47 \text{ nm}$ line [61] matches a hydrino transition predicted by Eqs. (20) and (25). The predicted 63.3 nm emission associated with dark matter was observed with the addition of hydrogen to a helium microwave plasma as shown previously [38-39] and in Figure 11. An alternative assignment suggested by Labov and Bowyer [61] is the 63.0 nm line of O V requiring a large-scale non-thermal source of ionization. Continuum radiation from transitions to low-level hydrino states can provide this radiation. Indeed, the observation of the 63.3 nm line is also associated with the presence of an interstellar X-ray background.

The first soft X-ray background was detected and reported [62] about 25 years ago. Quite naturally, it was assumed that these soft X-ray emissions were from ionized atoms within hot gases. Labov and Bowyer also interpreted the data as emissions from hot gases. However, the authors left the door open for some other interpretation with the following statement from their introduction:

“It is now generally believed that this diffuse soft X-ray background is produced by a high-temperature component of the interstellar medium. However, evidence of the thermal nature of this emission is indirect in that it is based not on observations of line emission, but on indirect evidence that no plausible non-thermal mechanism has been suggested which does not conflict with some component of the observational evidence.”

The authors also state that “if this interpretation is correct, gas at several temperatures is present.” Specifically, emissions were attributed to gases in three ranges: $5.5 < \log T < 5.7$; $\log T = 6$; $6.6 < \log T < 6.8$. Recent observations in the ultraviolet with HST and FUSE [63] and also XMM-Newton [64] confirm these extraordinary temperatures of diffuse intergalactic medium (IGM) and reveal that a large component of the baryonic matter of the universe is in the form of WHIM (warm-hot ionized media) [63-64]. The mysteries of the identity of dark matter, the observed dark interstellar medium spectrum, the source of the diffuse X-ray background, and the source of ionization of the IGM [63-64] are resolved by the formation of hydrinos that emit $q \cdot 13.6 \text{ eV}$ emission, EUV and X-ray continua depending on the state transition and conditions,

a 63.3 nm line [36-39], and pump the helium ion lines such as the 30.4 nm line. That the same transitions occur in stars [65] and the Sun as evident by corresponding continua and line emission in its spectrum resolves the solar corona problem, the cause of sunspots and other solar activity, and why the Sun emits X-rays [39].

C. Broadening of the Balmer α Line Widths. The Balmer α line profiles of the He/H_2 and H_2 plasma emission each comprised two distinct Gaussian peaks, an inner, narrower peak corresponding to a slow component with an average hydrogen energy of <1 eV and an outer, broader peak corresponding to a fast component. The slow population is assigned to thermal excitation in the plasma and matches those reported previously [15-22, 57, 66-78]. The Langmuir-probe determined electron density and temperature T_e were $10^9 - 10^{10} \text{ cm}^{-3}$ and 1 eV , respectively, that were consistent with reported Langmuir probe measurements for the n_e electron density n_e for the capacitively coupled RF, glow discharge, inductively coupled RF, and microwave plasma cells that showed selective, excessive fast H were $10^{10} - 10^{11} \text{ cm}^{-3}$ [71-72], $10^9 - 10^{11} \text{ cm}^{-3}$ [66], 10^9 cm^{-3} [79], and $<10^9 \text{ cm}^{-3}$ [18], respectively. Given the low electron density and temperature are the elimination of all other mechanisms [15-22] the extraordinarily broadened component is accepted to be due Gaussian Doppler due to a corresponding population of H with high kinetic energy [15-22, 57, 66-78]. The fast component was assigned to resonance kinetic energy transfer during the hydrino transition reaction with the elimination of the only alternative mechanism, electric field acceleration as the source of the energy of the extraordinarily fast H.

The axial scan of the 656.3 nm Balmer α line width recorded on a 1 Torr He/H_2 (95/5%) DC plasma discharge with needle-like electrodes at 400 V and 20 mA is shown in Figure 12. 50% of the hydrogen was “hot” with an average hydrogen atom energy of 45 eV, compared to <1 eV for the slow population. The intensity, but not the broadening, changed with position in the cell indicating that the broadening was not dependent on the electric field. In contrast, no broadening of the 667.816 nm He I line width was observed for 1 Torr He/H_2 (95/5%) at 400 V and 20 mA as shown in Figure 13. Similarly, 50% of the hydrogen was “hot” with an average hydrogen atom energy of 45 eV, compared to <1 eV for the slow population as shown by, the 656.3 nm Balmer α line width recorded on a 1 Torr H_2 DC plasma discharge with needle-like electrodes at 400 V and 20 mA (Figure 14). As in the case of the He/H_2 , there was no position dependency and thus, no field dependence of the broadening. The results of the 656.3 nm Balmer α line measurements, recorded as a function of position in the cell, direction relative to the electric field, strength of the electric field, and pressure from He/H_2 (95/5%) DC glow-discharge plasmas with needle electrodes supports the conclusion that field-acceleration models (FAM) are not valid to explain selective broadening in hydrogen-mixed plasmas. The reflector capabilities of the cathode that are necessary to explain the symmetrical profile in FAMs was removed by using needle-like electrodes. Even though the ability was removed for the cathode to reverse the axial kinetic energy gained by positive ions from acceleration along the field, the peak shape remained symmetrical. Furthermore, the role of the gas matrix as a reflector or divertor to randomize the direction of the electric-field-acquired kinetic energy was disproved. The gas pressure was varied more than three-orders of magnitude. The nondirectional, isotropic peak shape remained the same. The broadening was observed throughout the cell and was independent of angle with respect to the field; thus, it did not depend

on the field strength. This further failure of FAMs was confirmed by directly varying the applied voltage and observing no effect on the broadening. The broadening was only observed for helium mixed plasmas, but not for xenon. Selective, excessive H broadening with He/H_2 shown in this study and in other cell-types [16-18, 21] is not predicted with any FAM. However, the hydrino reaction with energy release that produces broadening of H that is time dependent [16, 20, 22,], nondirectional, position independent, selective to H, Gaussian Doppler, often two orders of magnitude in excess of the electron temperature, and specific to plasmas with atomic hydrogen and a catalyst (He^+ and $2H$ in this study) including those formed chemically [25-31, 40-43] explains the data in total. The predicted fast H due to the hydrino transition reaction was observed.

Intense hydrogen emission was also observed from capacitively coupled radio frequency (rf) water vapor plasmas in a static mode (no-flow condition); thus, it may strongly support the $2H$ catalyst reaction given by Eqs. (16-18). In addition, atomic and ionic oxygen emission was observed. For oxygen several chemical reactions fulfill the catalyst criterion. The bond energy of the oxygen molecule is 5.165 eV, and the first, second, and third ionization energies of an oxygen atom are 13.618 eV, 35.117 eV, and 54.9935 eV respectively [80]. The reactions $O_2 \rightarrow O + O^{2+}$, $O_2 \rightarrow O + O^{3+}$, and $2O \rightarrow 2O^+$ provide a net enthalpy of about 2, 4, and 1 times E_h respectively. In this regard, water vapor plasma was used as a source of H_2 , and H and O atoms to explore the possible catalytic reactions.

From the width of the emitted 656.3 nm Balmer α line, two populations of atomic hydrogen were present. As shown in Figures 15 and 16, a typical slow population was observed that was independent of time, and a new phenomenon, an extraordinary fast population (130–150 eV) was also observed that increased to a significant portion of the Balmer α emission with time, typically a period of 3–4 hours at moderate rf power levels. This is in complete contrast to the flow condition where hot H atoms had energies in the range of 2–3 eV. Experiments on the energy of hydrogen atom were also performed to study the effect of controlled addition of oxygen to a hydrogen plasma. It was found that the addition of O_2 decreased the broadening. This largely eliminates oxygen species as the catalyst. It directly rules out O_2 , and also largely eliminates $2O$ since hot H can collide with O_2 to form $2O$ as a binary reaction compared to a very less kinetically favorable ternary reaction in the case of O atoms. Confirmation of $2H$ as the catalyst was further provided by the results of maintaining a pure hydrogen plasma under batch conditions that closely matched those of the batch water vapor RF plasma. As shown in Figures 17a-b, a typical slow population was observed that was independent of time, and an extraordinary fast population (>100 eV) was also observed that increased to a significant portion of the Balmer α emission with time, typically a period of 3–4 hours at moderate rf power levels.

$2H$ was identified as the catalyst wherein atomic H initially forms on the cathode surface to initiate the catalysis reaction. Fast H in the gas phase advanced the rate, and in addition to H, hydrinos undergoing increasingly energetic transitions to lower states increased the energy of the fast H. This mechanism, completely consistent with the data, was extensively tested. Wide parameter regimes were explored for water vapor plasmas in the flow condition to replicate the excessive line broadening obtained in the no-flow condition. The catalyst mechanism was confirmed by Langmuir-probe measurements of plasma density and electron temperature, rf current and voltage measurements to characterize the plasma, studies on additional catalyst Ar^+ with hydrogen mixtures, and control studies on xenon-hydrogen

mixtures. As reported previously [20], Stark broadening or acceleration of charged species due to high electric fields cannot explain the results since (i) the electron density was low with a single bulk electron temperature of $\sim 2\text{--}3$ eV for all the plasma conditions, (ii) the rf field was constant with time including that of the plasma sheath, (iii) only the atomic hydrogen lines were broadened, (iv) the broadening was independent of the orientation of the fast H with respect to the field, (v) the fast H was found undiminished in regions of the cell without an electric field and at distances removed from the powered electrode more than an order of magnitude the thermalization distance, and (vi) catalyst-hydrogen mixtures showed extraordinary broadening in contrast to control non-catalyst plasmas that showed no broadening. The observation of time-dependent excessive Balmer line broadening in rf driven water vapor plasmas indicated the presence of an energetic reaction that meets the requirement of a source of Doppler energy other than that provided by the electric field. Water vapor plasmas were found to support a high rate of the $2H$ catalyst reaction wherein the predicted fast H due to the hydrino transition reaction was observed. Similar results were also observed when Ar^+ served as the catalyst as predicted and reported previously [16-19, 21-22].

D. NMR of Product $H_2(1/4)$ from Liquid-Helium Trapped He/ H_2 Microwave Plasma Gases and Water-Vapor RF-Plasma Gases. The 1H NMR spectra on sealed samples of liquid-helium-condensable helium-hydrogen plasma gases and water-vapor plasma gases dissolved in $CDCl_3$ relative to tetramethylsilane (TMS) are shown in Figures 18 and 19. The solvent peak was observed at 7.26 ppm, the H_2 peak was observed at 4.62 ppm, the broad peak at 1.54 was due to H_2O , and a sharp singlet at 0.22 ppm (Figure 18) matched methane from hydrocarbon reforming to produce hydrogen. The only peak in the spectra that could not be assigned to common species was the broad singlet peak upfield of H_2 at 1.25 ppm that matched the theoretical position of $H_2(1/4)$. The solution-phase NMR of the LHe collected plasma gas provides a definitive test of the theoretically predicted chemical shift of $H_2(1/4)$. Using Eq. (27) and the experimental absolute resonance shift of TMS, -31.5 ppm [49-50], the predicted gas-phase shift of $H_2(1/4)$ is

$$\frac{\Delta B_T}{B} = -30.6 \text{ ppm} - (-31.5 \text{ ppm}) = 0.9 \text{ ppm} \quad (39)$$

which is very close to the observed shift of 1.25 ppm shown in Figures 18 and 19. No known common contaminant has a single singlet peaks at this position, the peak is distinguishable based on its large width, and this peak-position is also in good agreement with the 1H MAS NMR value of 1.13 ppm observed for $H_2(1/4)$ in solid $NaH * F$ and corresponding solution value of 1.2 ppm [15]¹. The large peak width in solution is indicative of strong interactions of $H_2(1/4)$ with the matrix. Applicable relaxation interactions of $H_2(1/4)$ with the solution that effect the line width such as nuclear magnetic dipole interactions due to high mobility and spin rotational interaction are given in Becker [85]. These results provide direct evidence of lower-energy-hydrogen that is likely the identity of dark matter.

¹ With additional data, the 1.25 peak reported previously [23] is reassigned to $H_2(1/4)$, and the other sharp singlet peaks are likely common contaminants: methane, ethane, acetone, methyl chloride, and methanol [81-84].

III. Conclusion

In this study, we made specific theoretical predictions based on the GUTCP and tested them with standard, easily interpretable experiments wherein experimental conditions and methods were determined for readily reproducing the results. Specifically, the characteristic signatures of the reaction involving a resonant, nonradiative energy transfer from otherwise stable atomic hydrogen to the catalysts He^+ and $2H$ capable of accepting the energy to form hydrinos, $H(1/p)$, were sought. The catalyst energy transfer to pump the He^+ ion energy levels and increase the electron excitation temperature of H in helium-hydrogen and hydrogen plasmas was confirmed spectroscopically. In the former case, the pumping caused an inversion of the ion to atom line ratios, and in both cases, the $T_{excitation}$ was extraordinarily high, 2.5 eV to 3 eV, a factor of three increase over the typical temperature. For both catalysts, the energy due to the electron undergoing a radial transition to occupy a state of nearer radius was observed spectroscopically as a characteristic EUV continuum with a cutoff at 22.8 nm and extending to longer wavelengths. It was also observed as third-body kinetic energy wherein a resonant kinetic energy transfer to form fast H was the source of extraordinary (>50 eV) Balmer α line broadening. The predicted molecular hydrino, $H_2(1/4)$, was observed at 1.25 ppm by solution NMR on gases collected from helium-hydrogen and water-vapor-assisted hydrogen plasmas and dissolved in $CDCl_3$. Thus, we report the experimental confirmation of all four predictions for transitions of atomic hydrogen to form hydrinos. These results have profound implications theoretically, scientifically, and technologically in that they (1) confirm GUTCP in the prediction of hydrinos, (2) directly disprove atomic theories such as the Schrödinger and Dirac equations based on the definition of $n=1$ as the ground state, the defined state below which it is impossible to go, as expected based on many physical failings and preexisting mathematical inconsistencies [1, 3-12], 3) offer resolution to many otherwise inexplicable celestial observations with (a) the identity of dark matter being hydrinos, (b) the hydrino-transition radiation being the radiation source heating the WHIM and behind the observation that diffuse $H\alpha$ emission is ubiquitous throughout the Galaxy requiring widespread sources of flux shortward of 912 Å, and (c) the energy and radiation from the hydrino transitions being the source of extraordinary temperatures and power regarding the solar corona problem, the cause of sunspots and other solar activity, and why the Sun emits X-rays [39], and (4) directly demonstrate a new field of hydrogen chemistry and a powerful new energy source that currently operates at over 50 kW with performance levels projecting superiority over other energy sources such as fossil-fuel and nuclear energy sources as shown in the first paper of this series of three [15].

References

1. R. Mills, *The Grand Unified Theory of Classical Quantum Mechanics*; October 2007 Edition, posted at <http://www.blacklightpower.com/theory/bookdownload.shtml>.
2. R. Mills, Y. Lu, "Fifth Force," submitted.
3. R. L. Mills, "Classical Quantum Mechanics," *Physics Essays*, Vol. 16, No. 4, December, (2003), pp. 433-498.
4. R. Mills, "Physical Solutions of the Nature of the Atom, Photon, and Their Interactions to Form Excited and Predicted Hydrino States," in press.
5. R. L. Mills, "Exact Classical Quantum Mechanical Solutions for One- Through Twenty-

- Electron Atoms,” Physics Essays, Vol. 18, (2005), pp. 321-361.
6. R. L. Mills, “The Nature of the Chemical Bond Revisited and an Alternative Maxwellian Approach,” Physics Essays, Vol. 17, (2004), pp. 342-389.
 7. R. L. Mills, “Maxwell’s Equations and QED: Which is Fact and Which is Fiction,” Vol. 19, (2006), pp. 225-262.
 8. R. L. Mills, “Exact Classical Quantum Mechanical Solution for Atomic Helium Which Predicts Conjugate Parameters from a Unique Solution for the First Time,” in press.
 9. R. L. Mills, “The Fallacy of Feynman’s Argument on the Stability of the Hydrogen Atom According to Quantum Mechanics,” Annales de la Fondation Louis de Broglie, Vol. 30, No. 2, (2005), pp. 129-151.
 10. R. Mills, “The Grand Unified Theory of Classical Quantum Mechanics,” Int. J. Hydrogen Energy, Vol. 27, No. 5, (2002), pp. 565-590.
 11. R. Mills, The Nature of Free Electrons in Superfluid Helium—a Test of Quantum Mechanics and a Basis to Review its Foundations and Make a Comparison to Classical Theory, Int. J. Hydrogen Energy, Vol. 26, No. 10, (2001), pp. 1059-1096.
 12. R. Mills, “The Hydrogen Atom Revisited,” Int. J. of Hydrogen Energy, Vol. 25, Issue 12, December, (2000), pp. 1171-1183.
 13. N. V. Sidgwick, *The Chemical Elements and Their Compounds*, Volume I, Oxford, Clarendon Press, (1950), p.17.
 14. M. D. Lamb, *Luminescence Spectroscopy*, Academic Press, London, (1978), p. 68.
 15. R. L. Mills, G. Zhao, K. Akhtar, R. Chang, J. He, Y. Lu, W. Good, B. Dhandapani, “Commercializable Power Source from Forming New States of Hydrogen,” to be submitted.
 16. R. Mills, K. Akhtar, B. Dhandapani, “Tests of Features of Field-Acceleration Models for the Extraordinary Selective H Balmer α Broadening in Certain Hydrogen Mixed Plasmas,” submitted.
 17. R. L. Mills, P. Ray, B. Dhandapani, R. M. Mayo, J. He, “Comparison of Excessive Balmer α Line Broadening of Glow Discharge and Microwave Hydrogen Plasmas with Certain Catalysts,” J. of Applied Physics, Vol. 92, No. 12, (2002), pp. 7008-7022.
 18. R. L. Mills, P. Ray, B. Dhandapani, J. He, “Comparison of Excessive Balmer α Line Broadening of Inductively and Capacitively Coupled RF, Microwave, and Glow Discharge Hydrogen Plasmas with Certain Catalysts,” IEEE Transactions on Plasma Science, Vol. 31, No. (2003), pp. 338-355.
 19. R. L. Mills, P. Ray, “Substantial Changes in the Characteristics of a Microwave Plasma Due to Combining Argon and Hydrogen,” New Journal of Physics, www.njp.org, Vol. 4, (2002), pp. 22.1-22.17.
 20. R. L. Mills, B. Dhandapani, K. Akhtar, “Excessive Balmer α Line Broadening of Water-Vapor Capacitively-Coupled RF Discharge Plasmas” Int. J. Hydrogen Energy, Vol. 33, (2008), pp. 802-815.
 21. R. Mills, P. Ray, B. Dhandapani, “Evidence of an Energy Transfer Reaction Between Atomic Hydrogen and Argon II or Helium II as the Source of Excessively Hot H Atoms in RF Plasmas,” Journal of Plasma Physics, (2006), Vol. 72, Issue 4, pp. 469-484.24.
 22. J. Phillips, C-K Chen, K. Akhtar, B. Dhandapani, R. Mills, “Evidence of Catalytic Production of Hot Hydrogen in RF Generated Hydrogen/Argon Plasmas,” International Journal of Hydrogen Energy, Vol. 32(14), (2007), 3010-3025.
 23. R. L. Mills, J. He, Y. Lu, M. Nansteel, Z. Chang, B. Dhandapani, “Comprehensive Identification and Potential Applications of New States of Hydrogen,” Int. J. Hydrogen

- Energy, Vol. 32(14), (2007), pp. 2988-3009.
24. R. Mills, J. He, Z. Chang, W. Good, Y. Lu, B. Dhandapani, "Catalysis of Atomic Hydrogen to Novel Hydrogen Species $H^-(1/4)$ and $H_2(1/4)$ as a New Power Source," *Int. J. Hydrogen Energy*, Vol. 32, No. 12, (2007), pp. 2573-2584.
 25. R. Mills, P. Ray, B. Dhandapani, W. Good, P. Jansson, M. Nansteel, J. He, A. Voigt, "Spectroscopic and NMR Identification of Novel Hydride Ions in Fractional Quantum Energy States Formed by an Exothermic Reaction of Atomic Hydrogen with Certain Catalysts," *European Physical Journal-Applied Physics*, Vol. 28, (2004), pp. 83-104.
 26. R. Mills and M. Nansteel, P. Ray, "Argon-Hydrogen-Strontium Discharge Light Source," *IEEE Transactions on Plasma Science*, Vol. 30, No. 2, (2002), pp. 639-653.
 27. R. Mills and M. Nansteel, P. Ray, "Bright Hydrogen-Light Source due to a Resonant Energy Transfer with Strontium and Argon Ions," *New Journal of Physics*, Vol. 4, (2002), pp. 70.1-70.28.
 28. R. Mills, J. Dong, Y. Lu, "Observation of Extreme Ultraviolet Hydrogen Emission from Incandescently Heated Hydrogen Gas with Certain Catalysts," *Int. J. Hydrogen Energy*, Vol. 25, (2000), pp. 919-943.
 29. R. Mills, M. Nansteel, and P. Ray, "Excessively Bright Hydrogen-Strontium Plasma Light Source Due to Energy Resonance of Strontium with Hydrogen," *J. of Plasma Physics*, Vol. 69, (2003), pp. 131-158.
 30. R. L. Mills, J. He, M. Nansteel, B. Dhandapani, "Catalysis of Atomic Hydrogen to New Hydrides as a New Power Source," *International Journal of Global Energy Issues (IJGEI)*, Special Edition in Energy Systems, Vol. 28, Nos. 2/3 (2007), pp. 304-324.
 31. H. Conrads, R. Mills, Th. Wrubel, "Emission in the Deep Vacuum Ultraviolet from a Plasma Formed by Incandescently Heating Hydrogen Gas with Trace Amounts of Potassium Carbonate," *Plasma Sources Science and Technology*, Vol. 12, (2003), pp. 389-395.
 32. J. Phillips, R. L. Mills, X. Chen, "Water Bath Calorimetric Study of Excess Heat in 'Resonance Transfer' Plasmas," *Journal of Applied Physics*, Vol. 96, No. 6, pp. 3095-3102.
 33. R. L. Mills, X. Chen, P. Ray, J. He, B. Dhandapani, "Plasma Power Source Based on a Catalytic Reaction of Atomic Hydrogen Measured by Water Bath Calorimetry," *Thermochimica Acta*, Vol. 406/1-2, (2003), pp. 35-53.
 34. R. Mills, B. Dhandapani, M. Nansteel, J. He, T. Shannon, A. Echezuria, "Synthesis and Characterization of Novel Hydride Compounds," *Int. J. of Hydrogen Energy*, Vol. 26, No. 4, (2001), pp. 339-367.
 35. R. Mills, B. Dhandapani, M. Nansteel, J. He, A. Voigt, "Identification of Compounds Containing Novel Hydride Ions by Nuclear Magnetic Resonance Spectroscopy," *Int. J. Hydrogen Energy*, Vol. 26, No. 9, (2001), pp. 965-979.
 36. R. Mills, B. Dhandapani, N. Greenig, J. He, "Synthesis and Characterization of Potassium Iodo Hydride," *Int. J. of Hydrogen Energy*, Vol. 25, Issue 12, December, (2000), pp. 1185-1203.
 37. R. L. Mills, P. Ray, "Extreme Ultraviolet Spectroscopy of Helium-Hydrogen Plasma," *J. Phys. D, Applied Physics*, Vol. 36, (2003), pp. 1535-1542.
 38. R. L. Mills, P. Ray, B. Dhandapani, M. Nansteel, X. Chen, J. He, "New Power Source from Fractional Quantum Energy Levels of Atomic Hydrogen that Surpasses Internal Combustion," *J Mol. Struct.*, Vol. 643, No. 1-3, (2002), pp. 43-54.

39. R. Mills, P. Ray, "Spectral Emission of Fractional Quantum Energy Levels of Atomic Hydrogen from a Helium-Hydrogen Plasma and the Implications for Dark Matter," *Int. J. Hydrogen Energy*, Vol. 27, No. 3, (2002), pp. 301-322.
40. R. L. Mills, P. Ray, "A Comprehensive Study of Spectra of the Bound-Free Hyperfine Levels of Novel Hydride Ion $H^{-}(1/2)$, Hydrogen, Nitrogen, and Air," *Int. J. Hydrogen Energy*, Vol. 28, No. 8, (2003), pp. 825-871.
41. R. Mills, "Spectroscopic Identification of a Novel Catalytic Reaction of Atomic Hydrogen and the Hydride Ion Product," *Int. J. Hydrogen Energy*, Vol. 26, No. 10, (2001), pp. 1041-1058.
42. R. Mills, P. Ray, R. M. Mayo, "CW HI Laser Based on a Stationary Inverted Lyman Population Formed from Incandescently Heated Hydrogen Gas with Certain Group I Catalysts," *IEEE Transactions on Plasma Science*, Vol. 31, No. 2, (2003), pp. 236-247.
43. R. L. Mills, P. Ray, "Stationary Inverted Lyman Population Formed from Incandescently Heated Hydrogen Gas with Certain Catalysts," *J. Phys. D, Applied Physics*, Vol. 36, (2003), pp. 1504-1509.
44. R. Mills, P. Ray, R. M. Mayo, "The Potential for a Hydrogen Water-Plasma Laser," *Applied Physics Letters*, Vol. 82, No. 11, (2003), pp. 1679-1681.
45. R. L. Mills, P. C. Ray, R. M. Mayo, M. Nansteel, B. Dhandapani, J. Phillips, "Spectroscopic Study of Unique Line Broadening and Inversion in Low Pressure Microwave Generated Water Plasmas," *J. Plasma Physics*, Vol. 71, Part 6, (2005), pp. 877-888.
46. R. L. Mills, *The Grand Unified Theory of Classical Quantum Mechanics*, November 1995 Edition, HydroCatalysis Power Corp., Malvern, PA, Library of Congress Catalog Number 94-077780, ISBN number ISBN 0-9635171-1-2, Chp. 22.
47. F. Bournaud, P. A. Duc, E. Brinks, M. Boquien, P. Amram, U. Lisenfeld, B. Koribalski, F. Walter, V. Charmandaris, "Missing mass in collisional debris from galaxies," *Science*, Vol. 316, (2007), pp. 1166-1169.
48. B. G. Elmegreen, "Dark matter in galactic collisional debris," *Science*, Vol. 316, (2007), pp. 32-33.
49. K. K. Baldridge, J. S. Siegel, "Correlation of empirical $\delta(\text{TMS})$ and absolute NMR chemical shifts predicted by ab initio computations," *J. Phys. Chem. A*, Vol. 103, (1999), pp. 4038-4042.
50. J. Mason, Editor, *Multinuclear NMR*, Plenum Press, New York, (1987), Chp. 3.
51. C. Suarez, E. J. Nicholas, M. R. Bowman, "Gas-phase dynamic NMR study of the internal rotation in N-trifluoroacetylpyrrolidine," *J. Phys. Chem. A*, Vol. 107, (2003), pp. 3024-3029.
52. C. Suarez, "Gas-phase NMR spectroscopy," *The Chemical Educator*, Vol. 3, No. 2, (1998).
53. S. C. Badescu, P. Salo, T. Ala-Nissila, S. C. Ying, K. Jacobi, Y. Wang, K. Bedurftig, G. Ertl, "Energetics and vibrational states for hydrogen on Pt (111)," *Physical Review Letts.*, Vol. 88, No. 13, (2002), pp. 136100-1 to 136101-4.
54. A. D. Johnson, S. P. Daley, A. L. Utz, S. T. Ceyer, "The chemistry of bulk hydrogen: reaction of hydrogen embedded in nickel with absorbed CH_3 ," *Science*, Vol. 257, (1992), pp. 223-225.
55. R. Nieminen, "Hydrogen atoms band together," *Nature*, Vol. 356, (1992), pp. 289-291.
56. A. D. Johnson, K. J. Maynard, S. P. Daley, Q. Y. Yang, S. T. Ceyer, "Hydrogen embedded in Ni: production by incident atomic hydrogen and detection by high-resolution electron energy loss," *Physical Review Letters*, Vol. 67, No. 7, (1991), pp. 927-930.
57. E. L. Ayers and W. Benesch, *Phys. Rev.*, Vol. A37, (1988), p. 194.

58. J. Kikuchi, M. Suzuki, H. Yano, and S. Fujimura, Proceedings SPIE-The International Society for Optical Engineering, (1993), 1803 (Advanced Techniques for Integrated Circuit Processing II), pp. 70-76.
59. W. L. Wiese, *Plasma Diagnostics Technique*, Ed. R. H. Huddelstone and S. L. Leonard, Academic Press, New York, (1965), p. 265.
60. V. Grishin, B. Ishkhanov, S. Lichachev, V. Petukhov, "Electron Recirculator as High Efficiency Source of Hard Radiation," Proceedings of EPAC 2000, Vienna, Austria, (2000), 2606-2608.
62. S. Labov, S. Bowyer, "Spectral observations of the extreme ultraviolet background," *The Astrophysical Journal*, 371, (1991), pp. 810-819.
62. S. Bower, G. Field, and J. Mack, "Detection of an anisotropic soft X-ray background flux," *Nature*, Vol. 217, (1968), p. 32.
63. C. W. Danforth, J. M. Shull, "The low-z intergalactic medium. III. H I and metal absorbers at $z < 0.4$," *The Astrophysical Journal*, Vol. 679, (2008), pp. 194-219.
64. N. Werner, A. Finoguenov, J. S. Kaastra, A. Simionescu, J. P. Dietrich, J. Vink, H. Böhringer, "Detection of hot gas in the filament connecting the clusters of galaxies Abell 222 and Abell 223," *Astronomy & Astrophysics Letters*, Vol. 482, (2008), pp. L29-L33.
65. N. Craig, M. Abbott, D. Finley, H. Jessop, S. B. Howell, M. Mathioudakis, J. Sommers, J. V. Vallerga, R. F. Malina, "The Extreme Ultraviolet Explorer stellar spectral atlas," *The Astrophysical Journal Supplement Series*, Vol. 113, (1997), pp. 131-193.
66. M. Kuraica, N. Konjevic, "Line shapes of atomic hydrogen in a plane-cathode abnormal glow discharge," *Physical Review A*, Volume 46, No. 7, October (1992), pp. 4429-4432.
67. M. Kuraica, N. Konjevic, M. Platisa and D. Pantelic, *Spectrochimica Acta* Vol. 47, 1173 (1992).
68. I. R. Videnovic, N. Konjevic, M. M. Kuraica, "Spectroscopic investigations of a cathode fall region of the Grimm-type glow discharge," *Spectrochimica Acta, Part B*, Vol. 51, (1996), pp. 1707-1731.
69. S. Alexiou, E. Leboucher-Dalimier, "Hydrogen Balmer- α in dense plasmas," *Phys. Rev. E*, Vol. 60, No. 3, (1999), pp. 3436-3438.
70. S. Djurovic, J. R. Roberts, "Hydrogen Balmer alpha line shapes for hydrogen-argon mixtures in a low-pressure rf discharge," *J. Appl. Phys.*, Vol. 74, No. 11, (1993), pp. 6558-6565.
71. S. B. Radovanov, K. Dzierzega, J. R. Roberts, J. K. Olthoff, "Time-resolved Balmer-alpha emission from fast hydrogen atoms in low pressure, radio-frequency discharges in hydrogen," *Appl. Phys. Lett.*, Vol. 66, No. 20, (1995), pp. 2637-2639.
72. S. B. Radovanov, J. K. Olthoff, R. J. Van Brunt, S. Djurovic, "Ion kinetic-energy distributions and Balmer-alpha (H_α) excitation in $Ar - H_2$ radio-frequency discharges," *J. Appl. Phys.*, Vol. 78, No. 2, (1995), pp. 746-757.
73. G. Baravian, Y. Chouan, A. Ricard, G. Sultan, *J. Appl. Phys.*, Vol. 61, (1987), p. 5249.
74. A. V. Phelps, *J. Phys. Chem. Ref Data*, Vol. 21, (1992), p. 883.
75. C. Barbeau, J. Jolly, "Spectroscopic investigation of energetic atoms in a DC hydrogen glow discharge," *Journal of Physics, D, Applied Physics*, Vol. 23, (1990), pp. 1168-1174.
76. S. A. Bzenic, S. B. Radovanov, S. B. Vrhovac, Z. B. Velikic, and B. M. Jelenkovic, *Chem. Phys. Lett.*, Vol. 184, (1991), pp. 108-112.
77. E. L. Ayers, W. Benesch, "Shapes of atomic-hydrogen lines produced at a cathode surface," *Physical Review A*, Vol. 37, No. 1, (1988), pp. 194-199.

78. W. Benesch, E. Li, "Line shapes of atomic hydrogen in hollow-cathode discharges," *Optic Letters*, Vol. 9, No. 8, (1984), pp. 338-340.
79. D. Barton, J. W. Bradley, D. A. Steele, and R. D. Short, "Investigating radio frequency plasmas used for the modification of polymer surfaces," *J. Phys. Chem. B*, Vol. 103, (1999), pp. 4423-4430.
80. D. R. Lide, *CRC Handbook of Chemistry and Physics*, 79 th Edition, CRC Press, Boca Raton, Florida, (1998-1999), p. 9-55 and p. 10-175.
81. A. J. Gordon, R. A. Ford, *The Chemist's Companion: A Handbook of Practical Data, Techniques, and References*, John Wiley & Sons, Inc., (1972), pp. 256-270.
82. H. E. Gottlieb, V. Kotlyar, A. Nudelman, "NMR chemical shifts of common laboratory solvents as trace impurities," *J. Org. Chem.*, Vol. 62, (1997), pp. 7512-7515.
83. C.J. Pouchert, *Aldrich Library of NMR Spectra*, 2nd Ed., Aldrich Chemical Co. (1983).
84. C.J. Pouchert and J. Behnke, *Aldrich Library of ¹³C and ¹H FT-NMR Spectra*, 2nd Ed., Aldrich Chemical Co. (1993).
85. E. D. Becker, *High Resolution NMR Theory and Chemical Applications*, Second Edition, Academic Press, Inc., Orlando, (1980), pp. 20-22, 184-198.

Table 1. Summary of high-voltage pulsed plasma parameters to observe the EUV continuum from hydrino transitions.

Parameter	Experimental Conditions
Electron Beam Energy	1-2 kV
Electron Beam Pulse Duration	5-20 ms
Pulse Repetition Rate	5 Hz
Cathode Bias Voltage	12 kV
Helium/Hydrogen Mixture	98/2%
Gas Pressure	450 mTorr

Figure 1. Experimental setup for the high-voltage pulsed discharge cell.

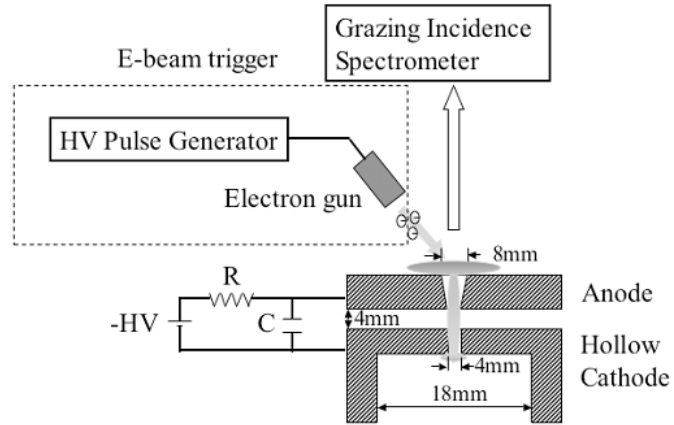


Figure 2. Schematic of the DC discharge created between the fine tips of 2% thoriated tungsten electrodes with the direction of axial scans defined. The cathode tip is taken as $z=0$ cm for side-on observations measured along the axis of the cathode from its tip to its electrical connection.

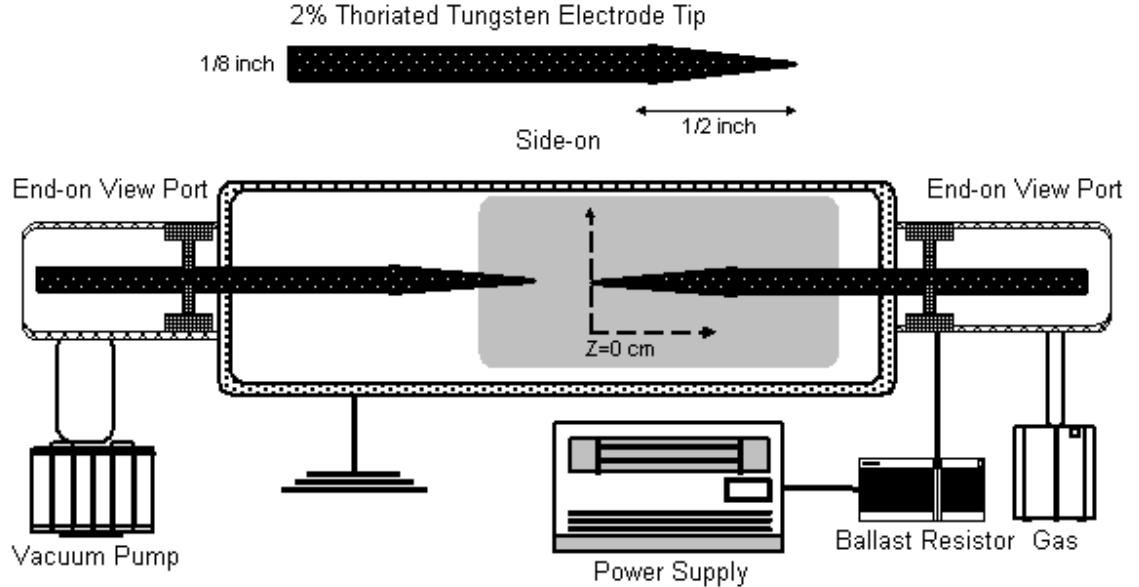


Figure 3. The experimental set up of a capacitively coupled rf plasma source.

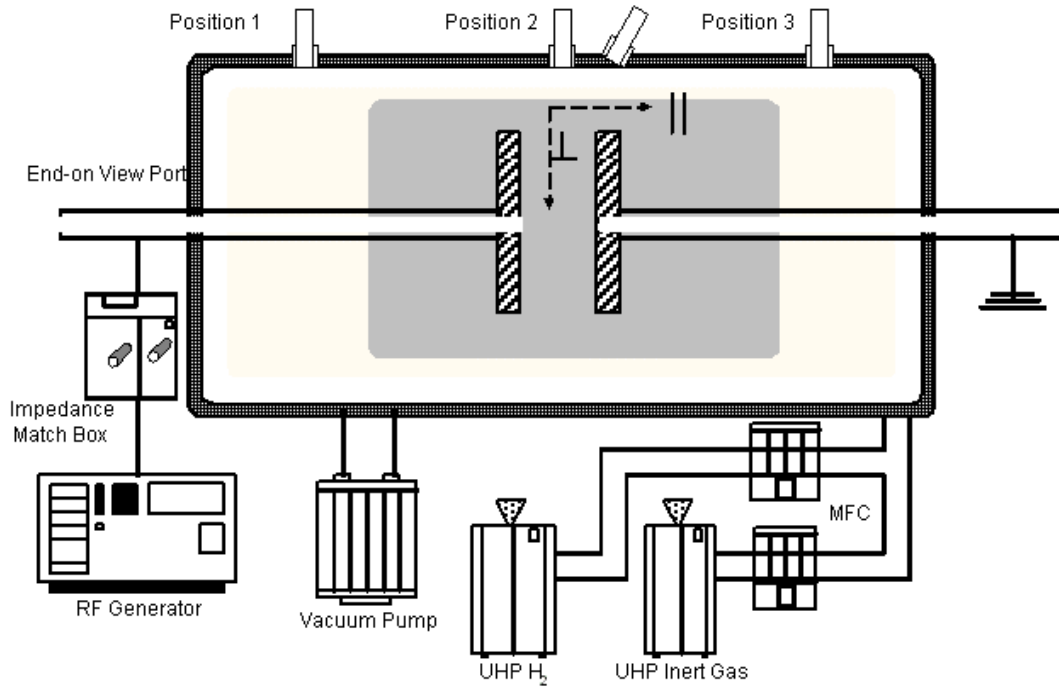


Figure 4. Control emission spectrum (25-60 nm) of the helium alone microwave plasma at 500 mTorr with a microwave power of 100 W recorded by the EUV grazing incidence spectrometer. Essentially, only the helium atomic lines were observed with the $1s^1 2p^1 \rightarrow 1s^2$ transition being dominant. The insert (20-45 nm region) shows the helium ion lines in the normal intensity ratios as a Rydberg series.

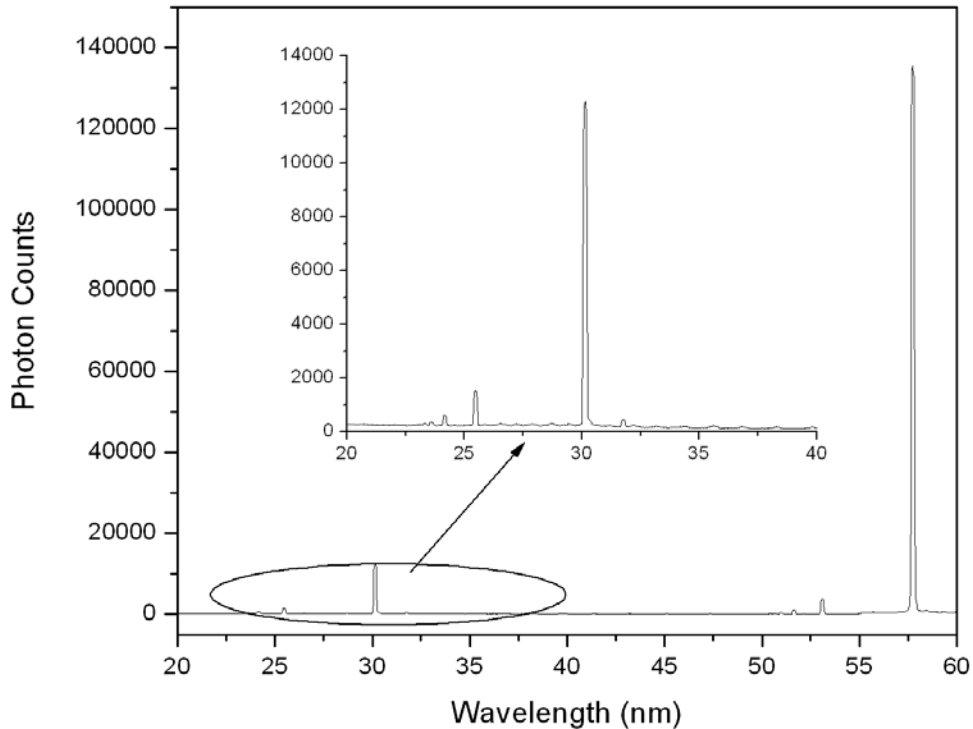


Figure 5. Emission spectra (20-60 nm) of helium-hydrogen mixture microwave discharge plasmas recorded by the EUV grazing incidence spectrometer. The hydrino transition reaction initiated by the addition of hydrogen was evidenced by the pumping of the He^+ lines. Specifically, the relative intensity of helium ion lines such as the 30.4 nm line increased with respect to helium atomic lines such as the 58.4 nm line as the hydrogen concentration was increased in the plasma. (a) 850 mTorr He + 50 mTorr H_2 with the microwave plasma at 40 W. (b) 750 mTorr He + 150 mTorr H_2 with the microwave plasma at 40 W.

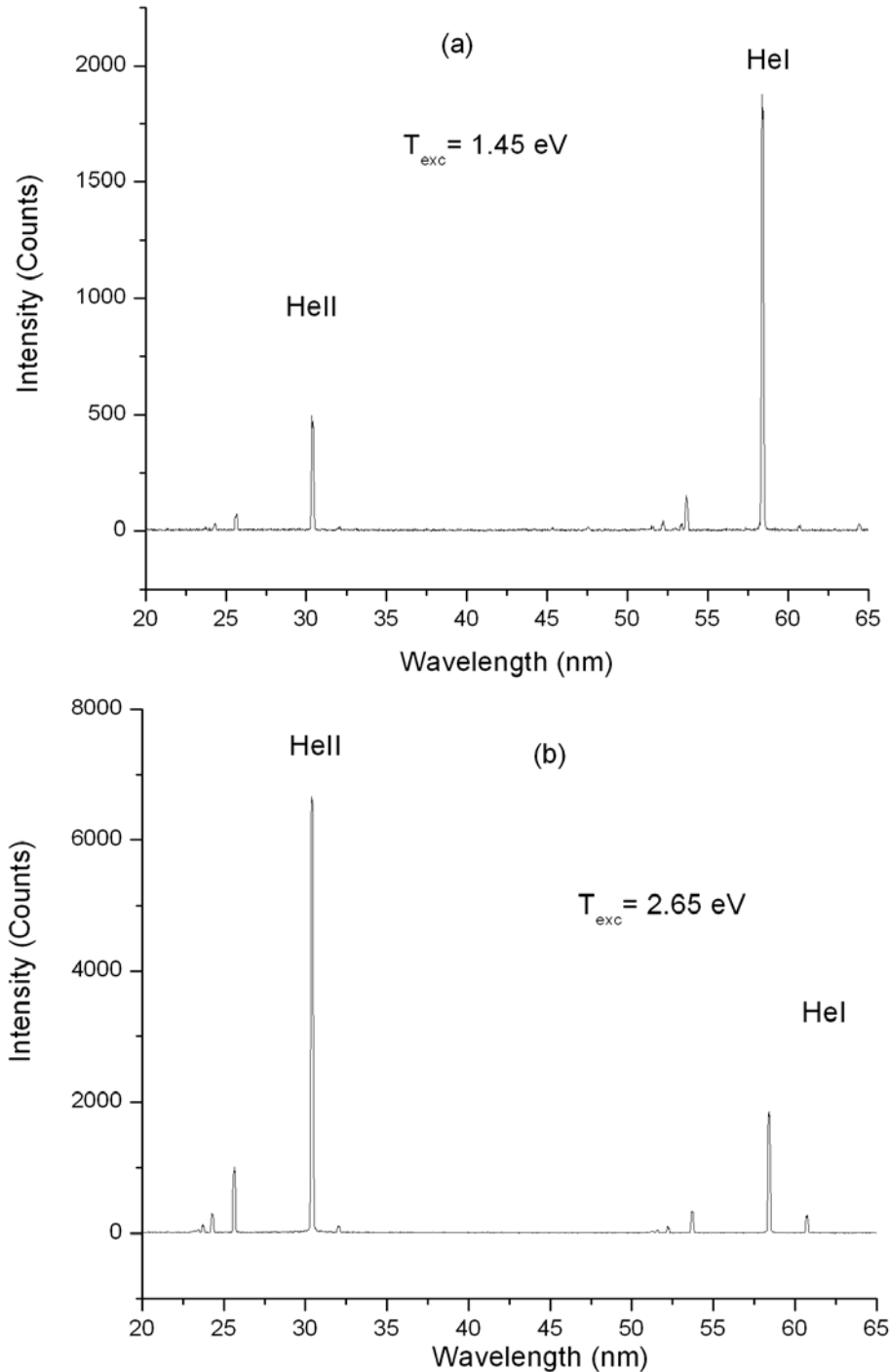


Figure. 6. Emission spectrum (370-660 nm) of a water-vapor microwave discharge plasma wherein the $2H$ catalyst served to maintain a high hydrino transition reaction rate as demonstrated by the pumping of the H lines to extraordinarily high levels. Specifically, the hydrogen Balmer lines corresponding to the transitions from the n th principal quantum level beyond the 16^{th} state to the $n=2$ level were observed.

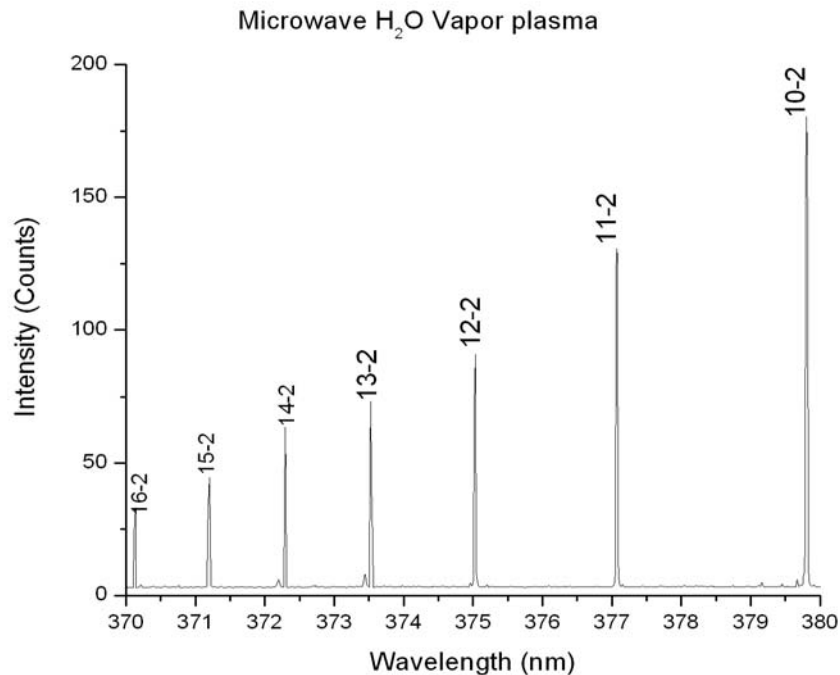


Figure 7. Emission spectrum (0-40 nm) of an electron-beam-initiated, high-voltage pulsed discharge in argon recorded by the EUV grazing incidence spectrometer. Only known argon atom and ion lines were observed in the absence of a continuum.

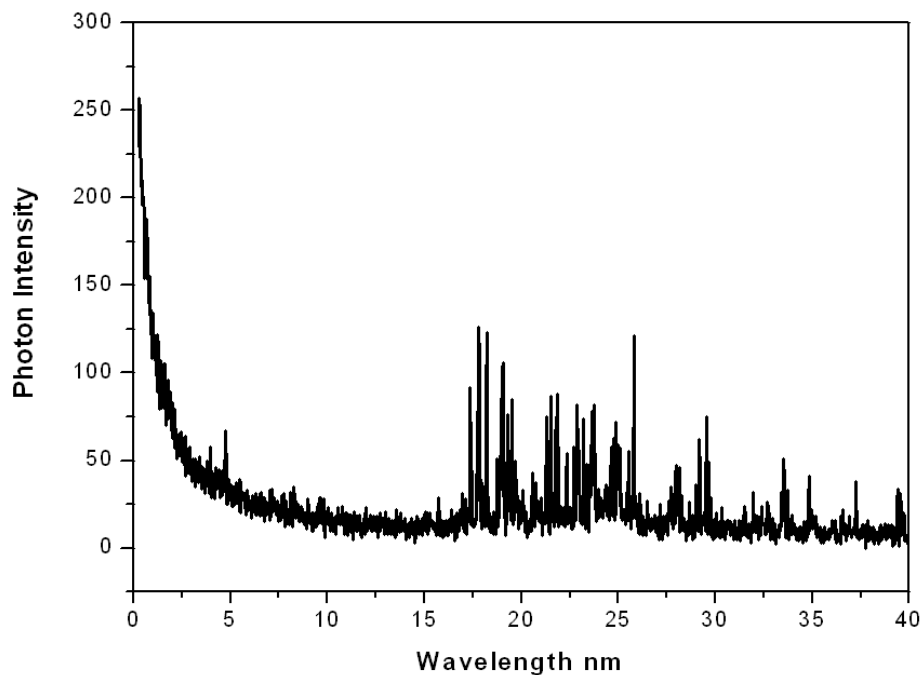


Figure 8. Emission spectrum (20-32 nm) of an electron-beam-initiated, high-voltage pulsed discharge in 900 mTorr helium 10 mTorr argon recorded by the EUV grazing incidence spectrometer. Only known helium ion lines were observed in the absence of a continuum.

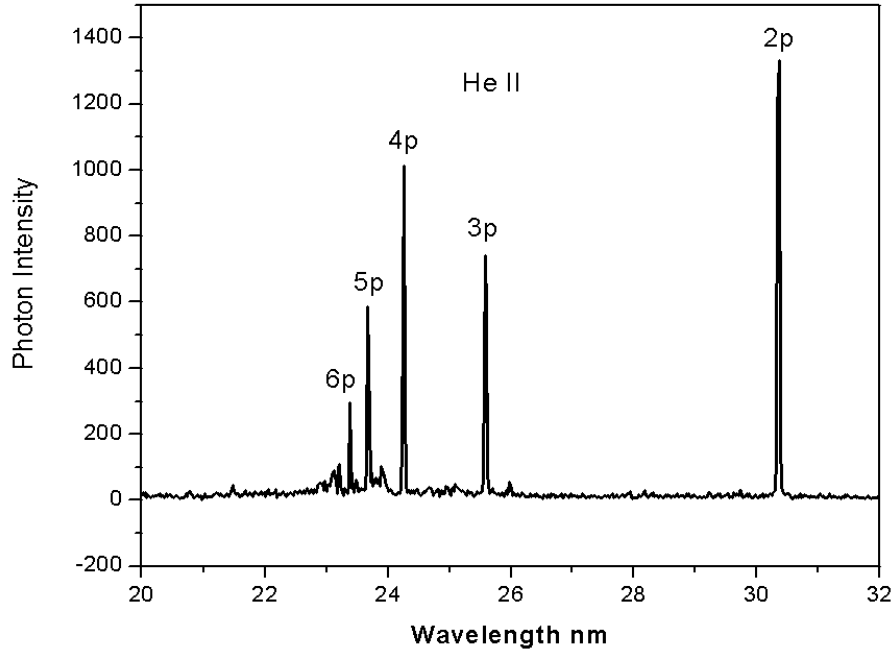


Figure 9. Emission spectrum (10-65 nm) of an electron-beam-initiated, high-voltage pulsed discharge in a helium-hydrogen mixture (98/2%), recorded by the EUV grazing incidence spectrometer. The predicted continua from the transition $H^* \left[\frac{a_H}{3} \right] \rightarrow H \left[\frac{a_H}{3} \right] + 54.4 \text{ eV}$ and

$H_{fast (KE=27.2 \text{ eV})} * \left[\frac{a_H}{4} \right] + \rightarrow H \left[\frac{a_H}{4} \right] + 40.8 \text{ eV}$ were observed.

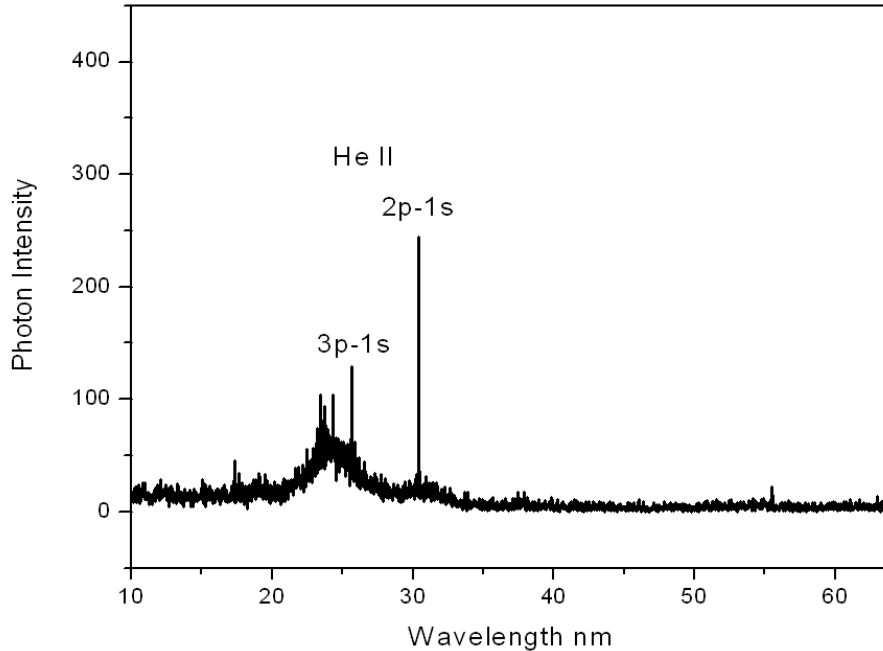


Figure 10. Emission spectrum (10-40 nm) of an electron-beam-initiated, high-voltage pulsed discharge in hydrogen, recorded by the EUV grazing incidence spectrometer. The predicted continuum from the transition $H^* \left[\frac{a_H}{3} \right] \rightarrow H \left[\frac{a_H}{3} \right] + 54.4 \text{ eV}$ was observed.

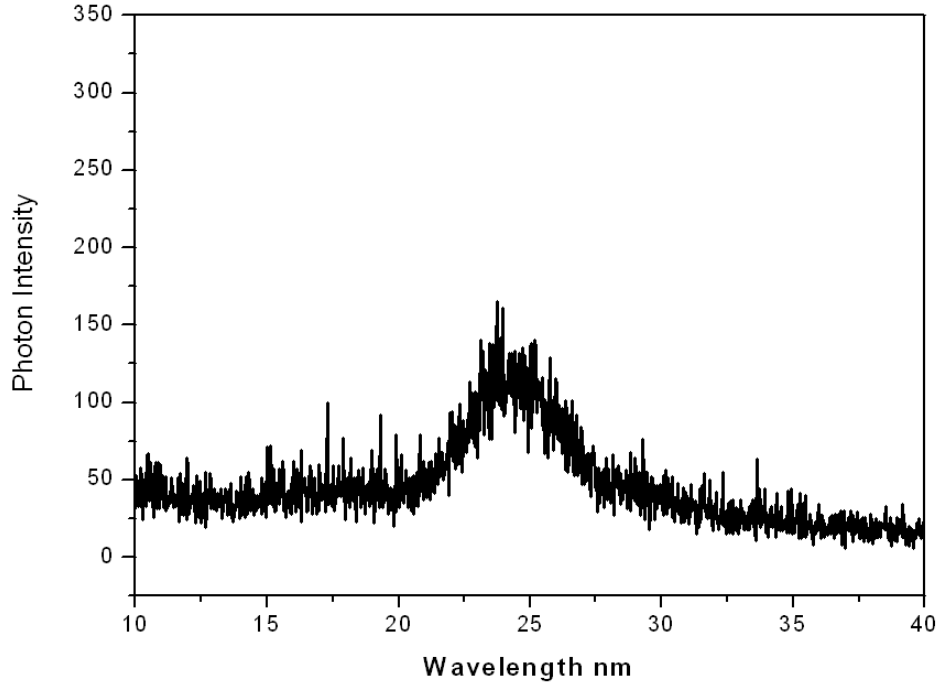


Figure 11. Emission spectrum (50-65 nm) of an electron-beam-initiated, high-voltage pulsed discharge in helium-hydrogen mixture (98/2%), recorded by the EUV grazing incidence spectrometer. The predicted 63.3 nm peak due to the excitation of the dominant transition of atomic helium by the energetic intermediate $H_{fast} (KE=27.2 \text{ eV}) * \left[\frac{a_H}{4} \right]$ was observed with the addition of hydrogen to a helium plasma.

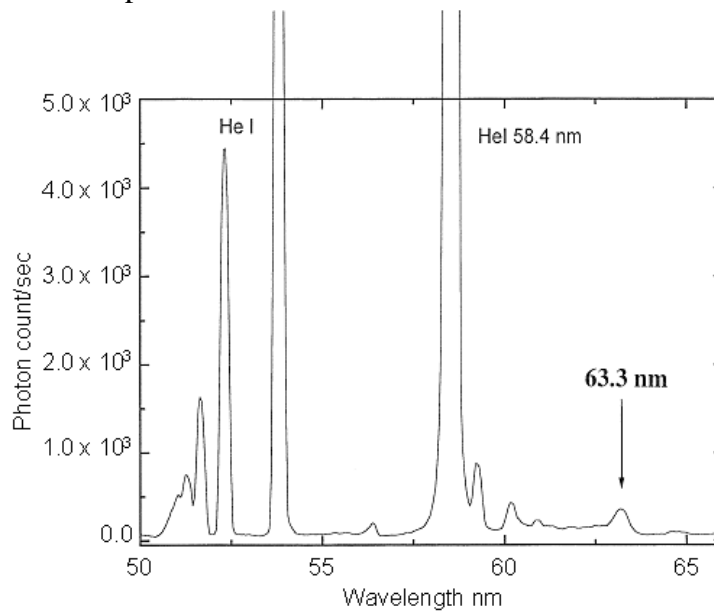


Figure 12. Axial scan of the 656.3 nm Balmer α line width recorded on a 1 Torr He/H_2 (95/5%) DC plasma discharge with needle-like electrodes at 400 V and 20 mA showing 50% of the hydrogen was 'hot' with an average hydrogen atom energy of 45 eV, compared to <1 eV for the slow population. The intensity, but not the broadening, changed with position in the cell indicating that the broadening was not dependent on the electric field.

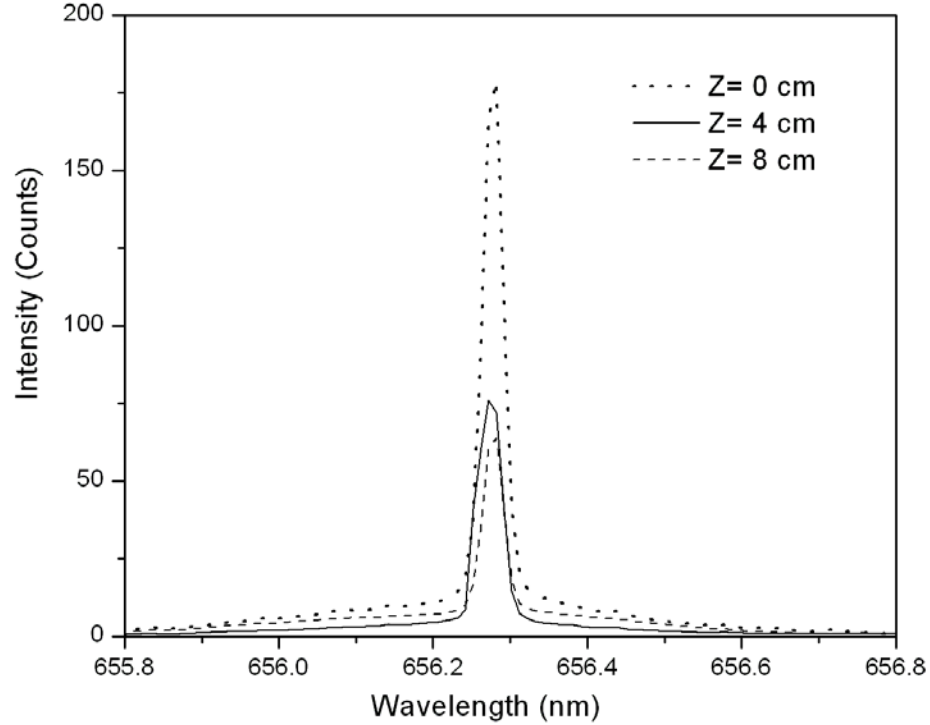


Figure 13. The 667.816 nm He I line width for 1 Torr He/H_2 (95/5%) at 400 V and 20 mA. No broadening was observed.

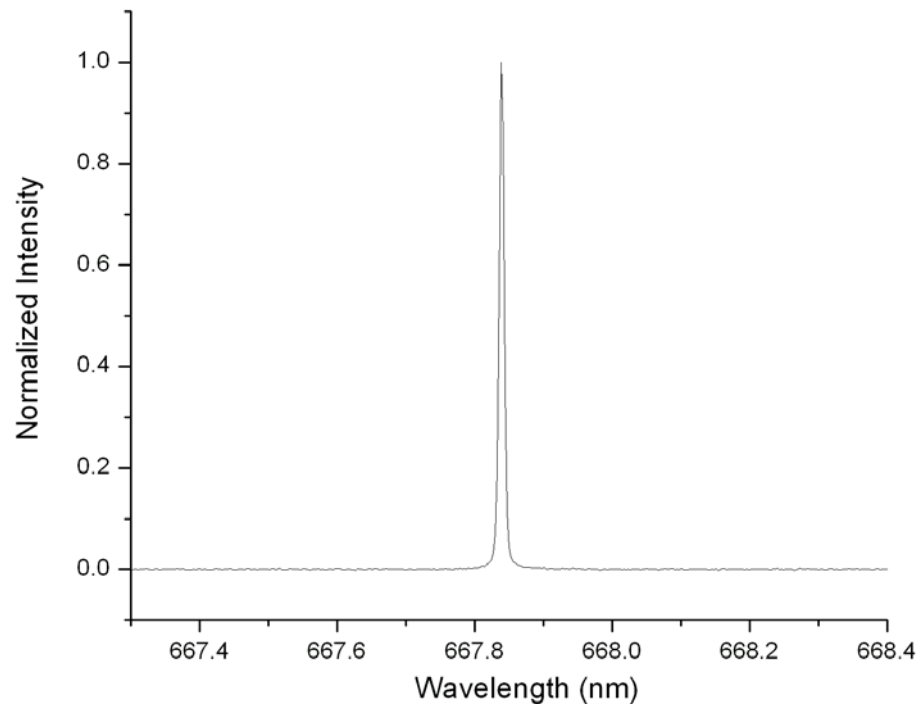
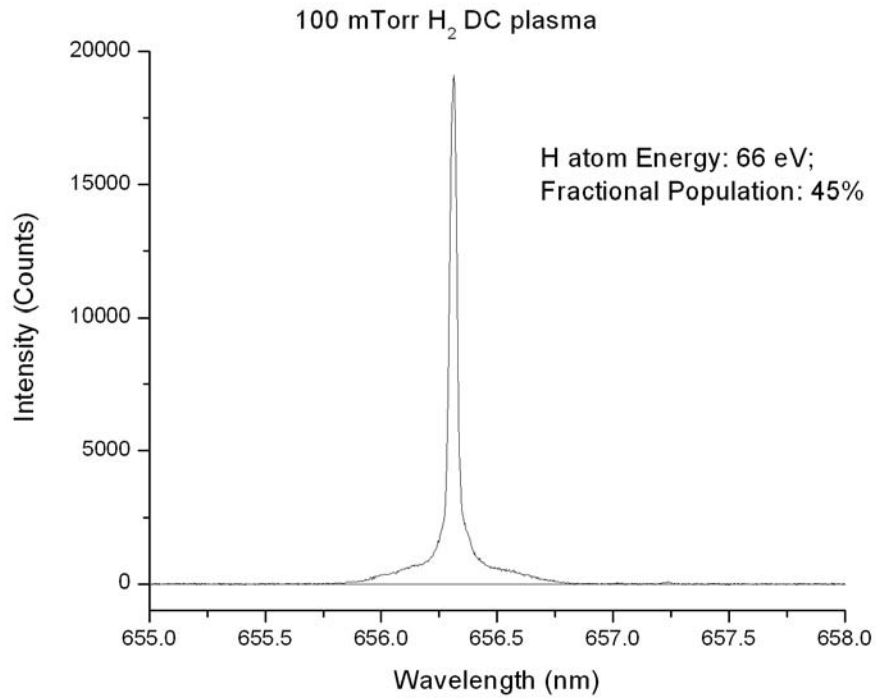


Figure 14. The 656.3 nm Balmer α line width recorded on a 1 Torr H_2 DC plasma discharge with needle-like electrodes at 400 V and 20 mA showing 45% of the hydrogen was 'hot' with an average hydrogen atom energy of 66 eV, compared to <1 eV for the slow population. The intensity, but not the broadening, changed with position in the cell indicating that the broadening was not dependent on the electric field.



Figurea 15a-b. The temporal evolution of Balmer α line profile width recorded on water-vapor plasmas at 100 mTorr and an rf coupled power of 200 Watt over a four-hour plasma duration: (a) The full peaks at matched maximum intensities. (b) The base of the emission profile showing the fast H population for water-vapor plasma. A fast population of H atoms with energies greater than 130 eV was observed later in time; whereas, only mildly warm H atoms with energies less than 5 eV was observed in the beginning of the experiment.

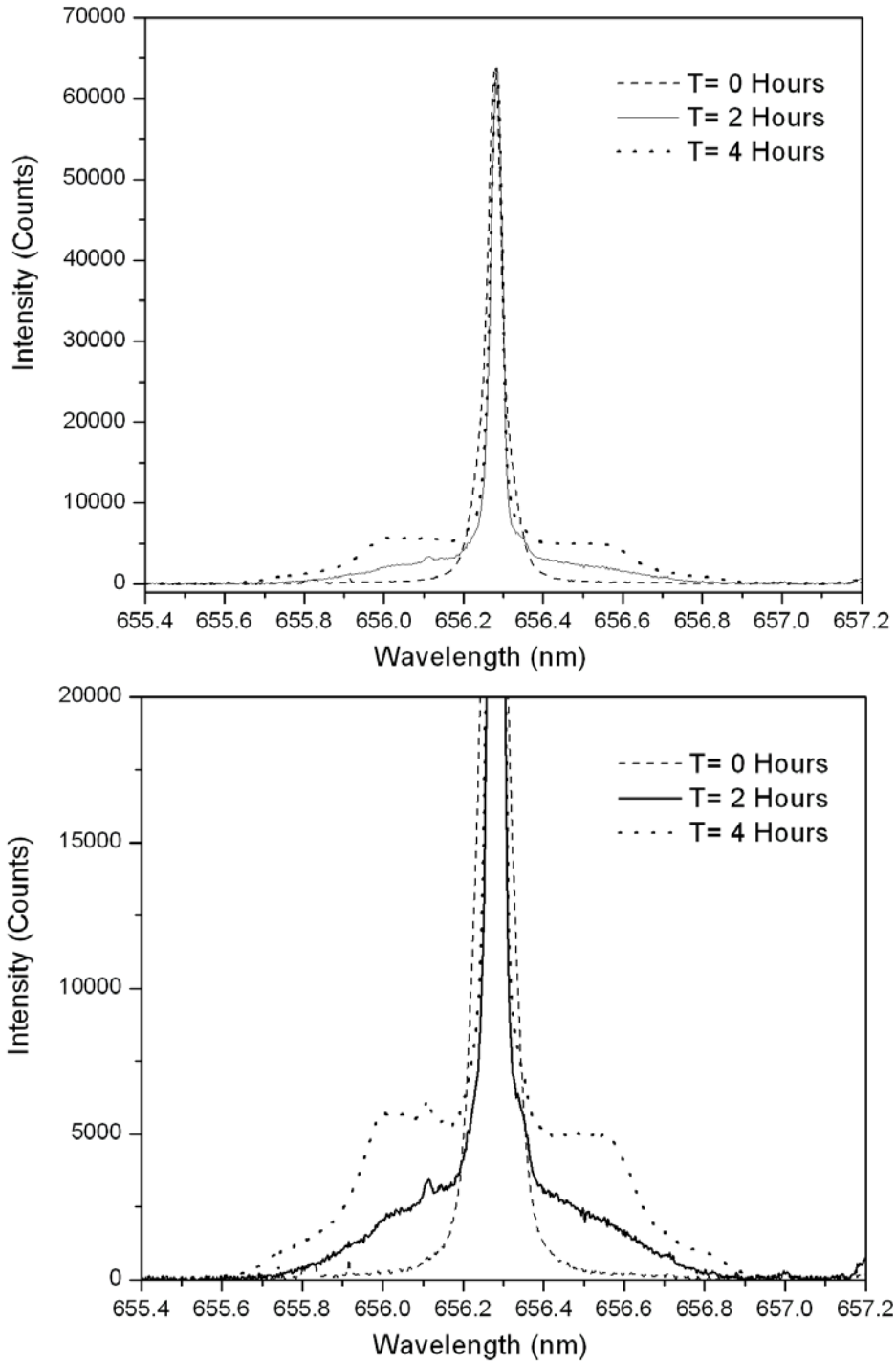
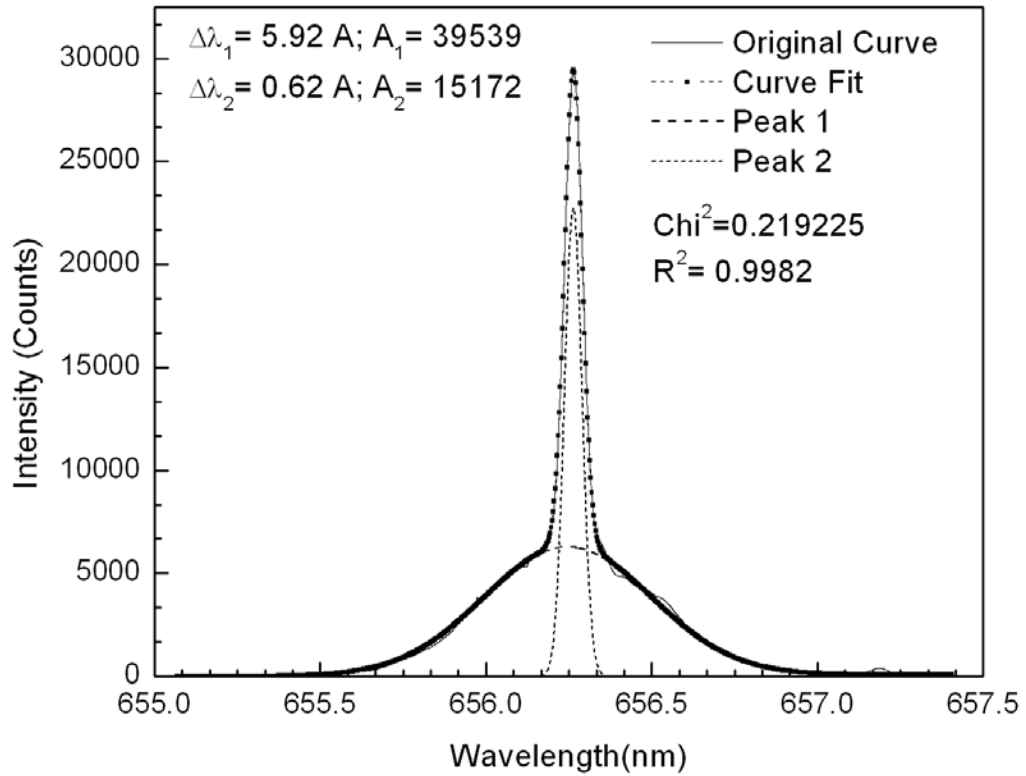
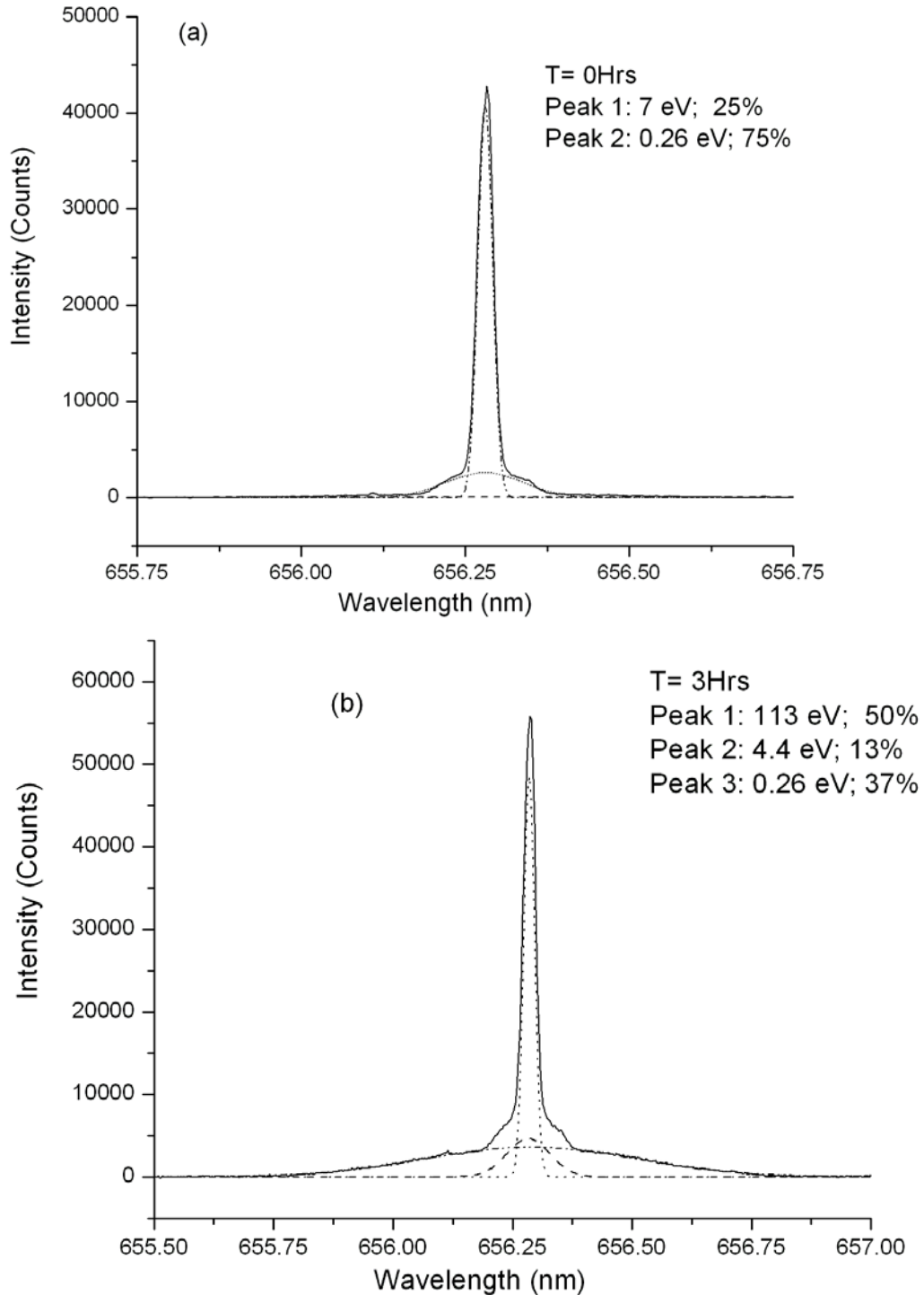


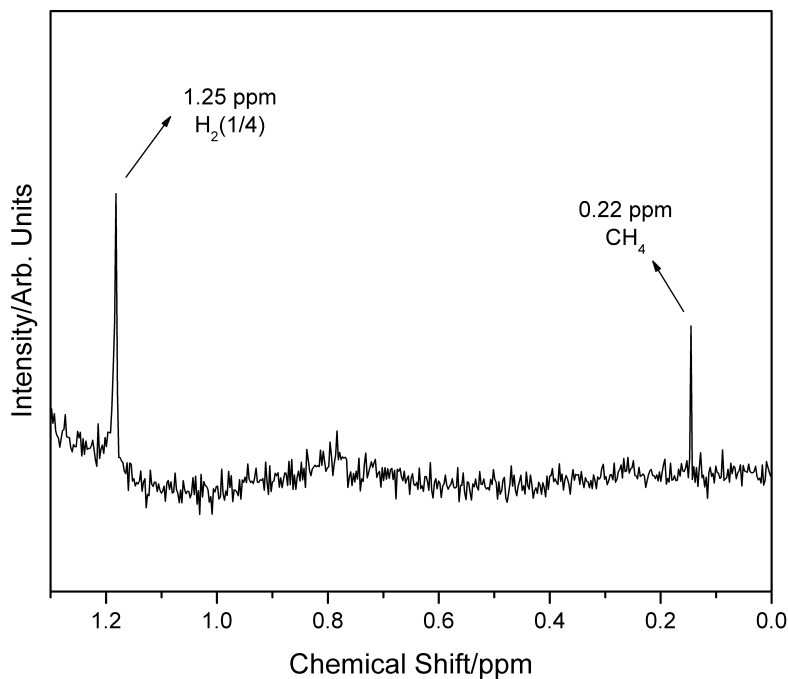
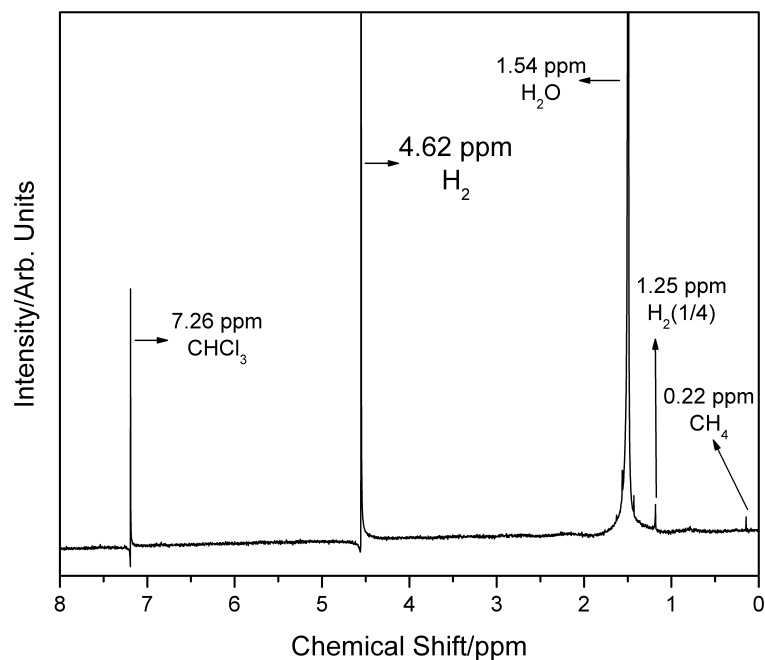
Figure 16. The statistical curve fit of the Balmer α line width profile recorded on water-vapor plasmas in the static mode (no-flow mode) after 4 hours at 100 mTorr and 200 W. The data best matched two Gaussian profiles having the $\chi^2 = \sum \frac{(Calculated - Measured)^2}{Calculated}$ and R^2 (correlation coefficient squared) values indicated. A fast population of 137 eV as well as a slow population of 1.5 eV were observed only for the water vapor plasmas.



Figures 17a-b. The temporal evolution of Balmer α line profile width recorded on hydrogen plasmas at 100 mTorr and an rf coupled power of 200 Watt over a three-hour plasma duration: (a) Initial populations showing only warm and cold hydrogen. (b) The emission profile showing the fast H population after 3 hours of maintaining the hydrogen plasma without flow. A fast population of H atoms with energies greater than 100 eV was observed later in time; whereas, only mildly warm H atoms with energies of 7 eV were observed in the beginning of the experiment.



Figures 18a-b. ^1H NMR relative to tetramethylsilane (TMS) of He/H_2 plasma gases collected at 4K and dissolved in CDCl_3 showing isolated $\text{H}_2(1/4)$ at 1.25 ppm. (a) 0 ppm to 8 ppm region showing the major peaks, the solvent peak at 7.26 ppm, the H_2 peak at 4.62 ppm, and the broad H_2O peak at 1.54 ppm. (b) 0 ppm to 1.3 ppm region showing the sharp CH_4 singlet at 0.22 ppm and a broad singlet peak upfield of H_2 at 1.25 ppm. The 1.25 ppm peak was the only peak in the spectrum that could not be assigned to common species. It matched the theoretical position of $\text{H}_2(1/4)$.



Figures 19a-b. ^1H NMR relative to tetramethylsilane (TMS) of water-vapor plasma gases collected at 4K and dissolved in CDCl_3 showing isolated $\text{H}_2(1/4)$ at 1.25 ppm. (a) 0 ppm to 8 ppm region showing the major peaks, the solvent peak at 7.26 ppm, the H_2 peak at 4.62 ppm, and the broad H_2O peak at 1.54 ppm. (b) 0 ppm to 4 ppm region showing a broad singlet peak upfield of H_2 at 1.25 ppm. The 1.25 ppm peak was the only peak in the spectrum that could not be assigned to common species. It matched the theoretical position of $\text{H}_2(1/4)$.

